ELSEVIER

Global and Planetary Change 25 (2000) 185–214

GLOBAL AND PLANETARY CHANGE

www.elsevier.com/locate/gloplacha

Modeling the effects of vegetation on Mediterranean climate during the Roman Classical Period: Part II. Model simulation

Oreste Reale *, Jagadish Shukla

Center for Ocean Land Atmosphere Studies, 4041 Powder Mill Rd., Suite 302, Calverton, MD 20705 USA

Received 9 July 1999; received in revised form 24 November 1999

Abstract

The purpose of this study is to perform a high-resolution general circulation model (GCM) experiment to quantify the sensitivity of regional climate to change in vegetation around the Mediterranean basin, corresponding to vegetation change during the Roman Classical Period (RCP), about 2000 years BP. First, an RCP vegetation distribution based on fossil pollen maps and historical records was defined. Second, the RCP vegetation inferred from palynology and other proxies was converted to the 12 vegetation types required by the biosphere model implemented in the GCM. The albedo change due to the change in vegetation significantly alters the atmospheric circulation over northern Africa and the Mediterranean. The consequences of this change involve a northward shift of the ITCZ in the African continent and a coupled circulation between northwestern Africa and the Mediterranean Sea. A large increase of precipitation occurs over the Sahel, the Nile valley and northwestern Africa. A smaller increase of precipitation occurs also over the Iberian Peninsula and the region corresponding to the south of the Caucasus range (Armenia). The increase of precipitation over northern Africa, the Iberian Peninsula and the Armenian region are consistent with the pollen, historical and geographical data. These results suggest that deforestation around the Mediterranean during the last 2000 years contributed to the dryness of the current climate.

Keywords: deforestation; desertification; vegetation history; land–atmosphere interaction; general circulation model; climate modeling

1. Introduction

In Part I of this study (Reale and Dirmeyer, 2000, hereafter RD), it was pointed out that during the Roman Classical Period (RCP, about 2000 years BP), northern Africa was moister than today (Grove, 1972) and that the Mediterranean region has been experiencing a continuous trend towards a "drier" (less water demanding) kind of vegetation. These assertions have been further supported by extensive reviews of climate history by Lamb (1977, 1982), proceedings of a symposium on the "Desertification of Europe" (Fantechi and Margaris, 1986; Mensching, 1986; Paepe, 1986; Van Overloop, 1986), and the multinational collection of "Case studies on Desertification" promoted by the United Nations Educational Scientific and Cultural Organization (Mabbutt and Floret, 1980). In addition to the review of climate history papers, Reale (1996) also exam-

* Corresponding author. Tel.: +1-301-902-1266; fax: +1-301-595-9793.

E-mail address: reale@cola.iges.org (O. Reale).

0921-8181/00/$ - see front matter
PII: S0921-8181(00)00003-5

ined the historical, geographical and archeological sources including classical literature and reports on agricultural productions that further support the notion of a climate change around the Mediterranean, and particularly of moister northern Africa during the RCP.

Among the several authors discussed in Reale (1996) and RD, the indirect evidence of moister northern Africa is found in the works of the Greek geographer and historian Strabo (64 BC–AD 21), who listed locations where vineyards and olive trees were widespread, stating also that the southern part of Roman Libya was the northern border of the desert. Moister conditions are suggested by the presence of elephants (indigenous over northwestern Africa at that time) as documented by Livy (59 BC–AD 17), and by Pliny the Elder (AD 23–79), who writes, in his 37-book "Natural History", about extensive forests, populated by elephants, in the south of the Atlas mountains. A diary from the geographer Ptolomaeus (AD 100–170), reported summer thunderstorms in Alexandria (Egypt), in contradiction with present climate. During the RCP and few centuries later, northern Africa was referred to as the "granary of Rome" and its cities, among the richest and most prosperous of the western world, display ruins of extensive aqueducts and public baths, suggesting larger water resources than today (RD).

Analysis of pollen data reinforces the notion that conditions were really different especially over northern Africa (Mehringer et al., 1979; Lippi et al., 1992). By combining palynology with the information provided by extant relict patches of vegetation, we reconstruct a continuous vegetation distribution for general circulation model (GCM) sensitivity study. Since all the vegetation environments are modern, we translated the maps into the 12 vegetation types (Table 1) in our biosphere model. Only the vegetation around the Mediterranean and along the Nile Valley is changed, since we want to isolate the signal due to land surface changes in this region. The experiment supports the idea that the vegetation distribution might have contributed to wetter conditions during the RCP.

Table 1
Vegetation types in SSiB

1	Broadleaf–evergreen trees (tropical or Mediterranean forest)
2	Broadleaf–deciduous trees
3	Broadleaf and needle-leaf trees (mixed forest)
4	Needle-leaf–evergreen trees
5	Needle-leaf–deciduous trees (larch)
6	Broadleaf trees with groundcover (savanna)
7	Groundcover only (perennial)
8	Broadleaf shrubs with perennial groundcover
9	Broadleaf shrubs with bare soil
10	Dwarf trees and shrubs with groundcover (tundra)
11	Bare soil
12	Winter wheat and broadleaf-deciduous trees (cultivated)

2. Vegetation history: the pollen method

Palynology provides a powerful tool to study past environments (Bell and Walker, 1992) and it is one of the most widely used proxy data sources for inferring past environmental conditions (Birks and Birks, 1980). Since the composition of the pollen rain reflects regional vegetation cover, fossil pollen obtained from undisturbed stratified sedimentarian sequences provides a record of vegetation change through time (Moore and Webb, 1978). Huntley and Birsk (1983) made an important contribution to the understanding of vegetation history over Europe. Huntley (1988) defined a new vegetation sequence of maps over Europe and the Middle East through time, since the Glacial Period, using the TWINSPAN code (Hill, 1979; Two Way Indicator Species Analysis), which classifies samples in a spatial–temporal array. These maps can be interpreted as maps of the domains of the major vegetational units, or associations, defined as ensembles of various *taxa* with different percentages. For example, a deciduous forest with oak (*Quercus*) being dominant, and with traces of birch tree, (*Fagus*), is classified as a different vegetational unit than one in which the birch is dominant and the oak is present in a smaller percentage.

In the history of vegetation described by Huntley (1988), it appears evident that, since the beginning of the Holocene (10,000 years BP), the forest vegetation spread rapidly across Europe as a response to the warming tendency, but different species moved in various directions with different speeds (15–50 km century^{-1}). Therefore, in the early Holocene, there are many vegetational units (i.e., associations

between species) which do not have an equivalent today, as a consequence of different migration rates, or different responses of the various species to the warming trend. However, according to the author, 3000-year BP vegetation can be finally defined as truly "modern", in terms of associations between species.

The prominent concern of Huntley's study was the large scale vegetational history since the ice age, and not the later, human induced vegetational changes; however, the author states that the impact of the Bronze Age, Iron Age, Roman, Medieval and modern times is reflected in the palynological record by evidence of the decreasing extent of woody vegetation and increasing amounts of herbaceous types, associated with human activity and agriculture. The tendency of vegetation depletion since historical times was observed in pollen by many other authors, interested in smaller scale studies. Of particular interest is Van Overloop's (1986) work, testifying to an abrupt shift from Mediterranean forest towards steppe in Greece in the centuries following the RCP.

Northern Africa vegetation history has not been described in as extensive manner as Huntley's work, although many pollen and paleovegetation studies have been performed for local sites, such as Lippi et al. (1992) and Mehringer et al. (1979) for Egypt, Ritchie (1987) for northwestern Sudan, Lezine and Bonnefille (1982) for Ethiopia. Ritchie and Haynes (1987), however, with a smaller database than Huntley's, provided a vegetation history for the eastern Sahara during the last 10,000 years. The authors found, in agreement with many other studies, that a major pluvial episode occurred between 9500 years BP and 4500 years BP in an area that the authors classify today as hyper-arid. The East Sahara was certainly much moister than present day. The retreat of that vegetation until its final disappearance is progressive and therefore, in the RCP, an intermediate vegetational situation between 4500 years BP and today was likely. An attempt to reconstruct the history of vegetation for western Africa was performed on a broader scale by Hooghiemstra (1988) from deep-sea core pollen records.

Also helpful for our study in northern Africa is the presence of relict forests in areas which today are almost completely steppe or even desert. Floret et al. (1980) in their desertification study of Tunisia, mention "remains in the mountains of primitive forests which have been cut by man" (forests dominated by *Pinus halepensis*), and "vestiges of wooded savanna with *Acacia raddiana* in the plains". The fact that scattered patches of forest or savanna can be considered as remains of a homogeneous cover allows us to obtain valuable information from the present vegetation where the pollen data are lacking.

3. The RCP vegetation

3.1. A possible RCP vegetation distribution

The RCP vegetation is a set of modern vegetational environments, the extent of which has been changing, but not the internal composition. Moreover, the temperature-dependent borders of various kinds of vegetational associations were very similar to the present ones, as the RCP phase was neither relatively colder nor warmer than the present phase.

Over continental Europe, the RCP vegetation is different from the modern only in terms of reduction of areas of vegetated land in favor of farmland or urban areas. Over southern Europe, northern Africa and the Middle East, the same process has occurred, but there is also a superposition of a "drying" trend: the domains characterized by more water demanding vegetational associations have been diminishing while those dominated by drier associations expanded.

The RCP vegetation we reconstructed is based on pollen maps (Huntley, 1990; Huntley and Birsk, 1983) wherever possible. For part of northern and eastern Africa, where less data were available, the criterion of extending the documented relict vegetation (Floret et al., 1980) over a geographically homogeneous landscape was followed, including any local pollen data available (Mehringer et al., 1979; Lezine and Bonnefille, 1982; Ritchie, 1987; Ritchie and Haynes, 1987; Lippi et al., 1992) and respecting the temperature constraints of the various types of vegetation. All the information available and the needed steps to build the most likely vegetational units distribution during the RCP are described in detail in Reale (1996). However, for the purpose of this work, this information is condensed into Tables 2 and 3, which associate to each vegetational environment its

Table 2
The RCP vegetational units

Veg. unit and/or prevalent species	Prevalent areas	MAP	*D*	Jan.	Jul.	F	SiB
Tropical forest Palms *Hyphaene thebaica* *Phoenix dactylifera*	LNV MP ND			$\gtrsim 10$	$\gtrsim 25$	n	1
Mediterranean forest: warmer type Evergreen oaks *Quercus suber, Q. ilex* Dwarf palms *Chamaerops humilis* Med. pines *Pinus halepensis, P. pinea* Olive tree *Olea europaea* spp.	CLT CPE CNWA WSCT	> 600	2	$\gtrsim 8$	$\gtrsim 25$	n	1
Mediterranean forest: cooler type Evergreen oak *Quercus ilex* Med. pines *Pinus pinea, P. halepensis* Olive tree *O. europaea* spp. Cypress *Cupressus sempervirens*	CLT CPE CNWA NCT	> 600	2	$\gtrsim 6$	$\gtrsim 24$	n	1
Deciduous forests with oak dominant *Quercus* sp. not *ilex* *Q. robur, Q. petrea, Q. cerris*	BI CEU PEI TP	> 600	1	$\gtrsim -1$	$\gtrsim 20$	y	2
Deciduous forests with beech dominant *Fagus* sp.	BM PEM CEU	> 1000	< 1	$\gtrsim -3$		y	2
Mixed deciduous/needle-leaf with beech *Fagus* sp., *Abies* sp., *Picea* sp.	A BM P	> 800	< 1	$\gtrsim -3$		y	3
Mixed deciduous/needle-leaf with oak *Quercus* sp. not *ilex*, *Pinus* sp. *P. nigra* spp.	BM SCM SCR TM WSCT ZM	> 600	1	$\gtrsim -1$		y	3
Mixed deciduous/needle-leaf with cedar *Cedarus* sp., *Quercus* sp. not *ilex*	AR LEM WSCT	> 600	2	$\gtrsim -1$		y	3
Evergreen needle-leaf (wetter type, northern and western domain) *Abies alba, Picea excelsa* *Pic. abies, Pic. omorica*	A BM P	> 800	< 1		$\lesssim 19$	y	4
Evergreen needle-leaf (drier type, southeastern and eastern domain) *Abies cephalonica, A. nordmanniana*	CPE ETM	> 600	3		$\lesssim 23$	y	4
Deciduous needle-leaf (*Larix*)	nc						5
Groundcover with isolated standing trees (Savanna) *Acacia raddiana, A. horrida, A. cavenia*	LNV MP SAR ST SU	> 300	10	$\gtrsim 10$	$\gtrsim 25$	n	6
Perennial herbaceous types only	MP					n	7
Mediterranean scrub	CLT	> 300	4	$\gtrsim 6$	$\gtrsim 24$	n	8
Groundcover with shrubs and no standing tree	CEG IP SU TP UNV	> 200					8
Shrubs with bare soil	SA	> 100					9

Table 2 (*continued*)

Veg. unit and/or prevalent species	Prevalent areas	MAP	*D*	Jan.	Jul.	F	SiB
Tundra	nc						10
Bare soil	SA	< 120					11
Agricultural land							12

The table is illustrated in the caption of Table 3, where the abbreviations of the areas are listed.

internal composition, domain, climate constraints and conversion into the vegetation types allowed by our biosphere model, SSiB (Xue et al., 1991). The listed climatic constraints are peculiar of the Mediterranean region, and might be slightly different over other areas. The 12 SSiB vegetation types are listed in Table 1. More than one vegetational unit can fit into the same SiB category. For example, over northern Africa and the Middle East there are some areas classified as tropical forest (dominated by palms like *Hyphaene thebaica* and *Phoenix dactylifera*). However, the so-called Mediterranean forest, a vegetational environment in which the dominant species are evergreen oaks like the *Quercus ilex* and *Q. suber*, dwarf palms (*Chamaerops humilis*), olive trees (*Olea europaea* spp.), mixed with Cypress *Cupressus. sempervirens* and Mediterranean pines *Pinus pinea*, *P. halepensis*, is regarded the same as tropical forest (RD), following Dorman and Sellers (1989).

Two kinds of broad leaf deciduous oak forest are typical of the Mediterranean region: the one dominated by deciduous oaks like *Quercus petraea*, *Q. robur*, *Q. cerris* (over most of the continental Iberian Peninsula, Italy, France and the Balkans) and, at higher altitudes, the one dominated by the beech tree (*Fagus sylvaticus*), much more water demanding (at least 1000 mm year^{-1}).

Similarly, three types of mixed broad-leaf/needle-leaf forests can be found (see Table 2) over the Mediterranean region. Particularly notable is the unit characterized by the cedar (*Cedarus* sp.), once widespread over the Mediterranean but particularly over the Lebanon mountains: Lebanon cedar forests were widely recorded in historical records as being the main source of wood for the Phoenician shipping industry. Presently, besides few patches of extant forest, the area is regarded as semi-desert or desert in the southern part (Israel and Jordan) and essentially farmland in the north (Lebanon and northwestern Syria).

3.2. The RCP vegetation for a GCM experiment

It was necessary to convert the information into a gridded form at the resolution required by our experiment (R40, approximately 2.8° longitude and 1.8° latitude). Since complex orography causes sharp environmental transitions on scales smaller than our gridboxes, the unit with the larger fractional area was assigned to each gridbox.

A good example is the domain of the Mediterranean forest over northern Africa. The Mediterranean forest needs mild and rainy winters with no persistent frost and can tolerate relatively dry summers and some droughts. The total rain required is at least 600 mm year^{-1}, of which a total 120 mm must fall during the months of June, July, August and September. With increasing height and lower temperatures, the Mediterranean forest leads to broadleaf deciduous or mixed deciduous needle-leaf, whereas with increasing aridity, the Mediterranean forest changes to groundcover with shrubs and isolated trees like the coark oak (*Quercus suber*), dwarf palms or some of the Mediterranean pines. This environment (Mediterranean scrub) has the same temperature constraints as the Mediterranean forest but demands less water (300 mm year^{-1}). Over Libya and Tunisia, the extent of the Mediterranean scrub in the RCP is estimated to be the extent of the Roman penetration; with a further increase of aridity this environment turns into groundcover with shrubs and no standing trees. All these transitions often occur over a distance of a few kilometers. Sharp transitions between vegetational environments occur also over Turkey, on the southern flank of the Cau-

Table 3
Areas listed in Table 2

Abbreviations	List of locations in Table 2
nc	not changed in the experiment
A	Alps
AR	Atlas range
BI	Balkanic (excluding Greece) interior
BM	Balkanic mountains
CEG	Coastal Egypt
CEU	Continental Europe
CLT	Coastal Libya–Tunisia
CPE	Coastal peninsular Europe (Iberia, Italy and Greece)
CNWA	Coastal north-western Africa
ETM	Eastern Turkish mountains
IP	Iranian plateau
LEM	Lebanon mountains
LNV	Lower Nile Valley
MP	Mesopotamia
NCT	Northern coastal Turkey
ND	Nile delta
P	Pyrenees
PEI	Peninsular Europe interior
PEM	Peninsular Europe mountains
UNV	Upper Nile Valley
SA	Sahara
SAR	Southern Atlas range
SCM	Southern Caspian mountains
SCR	Southern Caucasus range
ST	Southern Tunisia
SU	Sudan
TM	Taurus mountains
TP	Turkish plateau
WSCT	Western and Southern coastal Turkey
ZM	Zagros mountains

Table 2 explanation: In the first column, vegetation environments typical of the Mediterranean are listed. In the second column, the areas in which there is large evidence of those units in the RCP are listed. The following columns display some climatic constraints significant for this study: MAP (mean annual precipitation, in mm $year^{-1}$), D (tolerable number of non-freezing months with continuous drought), JAN and JUL (mean January and July temperature in °C), F (resistance to more than 72 hours of continuous frost). Climatic constraints that are not significant for our studies have not been listed. For example, the precipitation requirements for palm tree forests are not significant because most of the palm forest were located along rivers like the Nile, the Tigris and the Euphrates; so part of the needed water was provided by floods or by soil moisture. In the last column the conversion of RCP environments into SSiB vegetation types is provided.

casus mountains, on the mountainous areas to the south of the Caspian Sea and over the Zagros mountains. These areas are today farmland to a large extent but display evidence of past larger and diverse forest environments.

The result of all these analyses provides the vegetation map at the needed resolution. In Fig. 1, the R40 Control and RCP vegetation maps are displayed; 185 gridpoints were changed to create the RCP vegetation map.

4. Experiment design

The model used is the so-called COLA GCM (Kinter et al., 1988, 1997), with a rhomboidal truncation at wavenumber 40. The corresponding gaussian grid is approximately 2.8° longitude and 1.8° latitude, which allows a fairly realistic representation of geographical features. The R40 experiment was designed taking into account the RD results, which showed a significant change in rainfall due to the changes in vegetation in summer only. Therefore, instead of a long-term integration through many annual cycles, two sets (control and experiment) of five summer only integrations of 4 months each were performed. The initial conditions were set on June 1st for the years 1987, 1988, 1990, 1992 and 1993. The years were selected by looking at observed data, in order to represent a possible range of precipitation variability over northern Africa: 1990 was a relatively dry year on eastern Sahel and Sahara, 1992 was very wet, 1993 was wet in northwest Africa, but dry in the northeast, whereas 1987 and 1988 do not have any extreme. In order to obtain a more realistic variability, the R40 experiment was done with observed seasonally varying sea surface temperature (SST), instead of climatologically prescribed SST (RD).

The choice of adopting a higher resolution decreases the chance of making long-term integrations; therefore the assumption we make is that the signal might reach the same level of significance as in RD study, if we could perform a longer integration. The aim of this part of the study is mainly to focus on the dynamics of the response.

The vegetation change includes a slightly larger part of the Nile Valley (essentially in Sudan), compared to RD: an area inhabited by civilizations con-

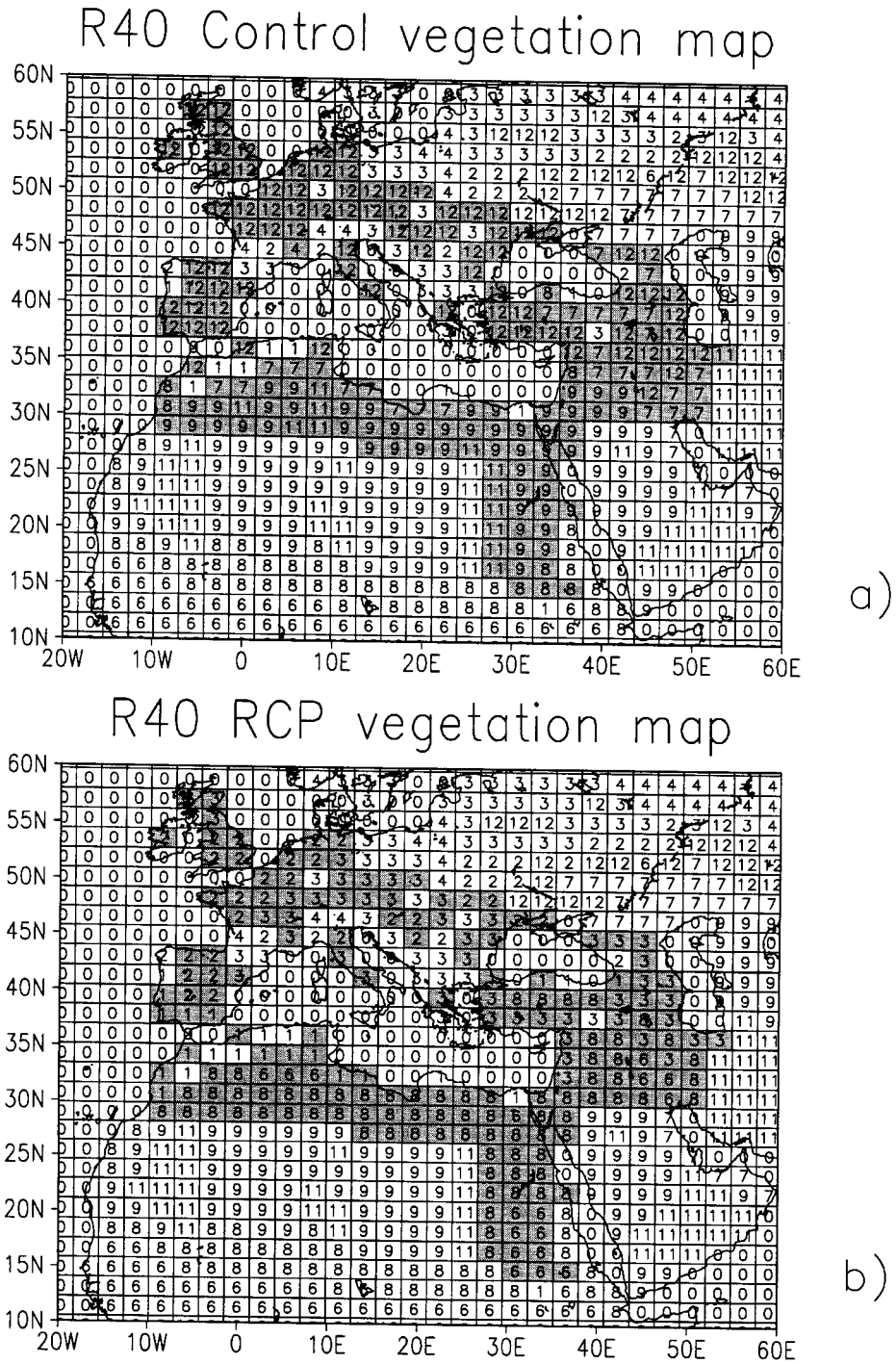

Fig. 1. Vegetation Map at R40 Resolution. The numbers correspond to the vegetation types and are listed in Table 1. Panel a: Control; Panel b: RCP. Shading indicates gridboxes where modern and RCP vegetation differ.

temporary to Rome (Nubia, Meroe and Ethiopia) that has been experiencing a desertification trend (Ritchie and Haynes, 1987). However, since we want to isolate the signal caused by different vegetation around the Mediterranean, the vegetation of the rest of the world is assumed to be the present one in both experiment and control. For the same reason, we do not include in our experiment other forcing-like changes in the solar constant or in the earth orbital parameters.

Unlike the RD experiment, which used Mintz and Walker (1993) soil moisture, this experiment was initialized with the ECMWF soil moisture, adopting the procedure described in Fennessy and Shukla (1999).

5. Results of the experiment

5.1. The precipitation

The integration with the present vegetation is referred to as the "Control" run, and the one with the RCP vegetation as the "Experiment" run. When displaying field differences between the two integrations, they will be referred to as (RCP-Control). Unlike the RD experiment, the transients in the soil moisture appear to be very short: only of about 1 month for each run, probably due to the better initialization. However, rigorously speaking, there is no way to initialize the model with the "right" RCP soil wetness.

Fig. 2 shows the global map of JAS control precipitation, averaged over the 5 years of integration (1987, 1988, 1990, 1992 and 1993) and the difference (RCP − Control). A zonal dipole pattern is detectable over central–northern Africa, with the positive areas larger than the negative ones, confirming a shift and a strengthening of the ITCZ during the JAS period. Gridpoints attaining the 95% or greater significance level using the t-test outline an area over which the precipitation increase (RCP − Control) is significant: essentially most of northern and northeastern Africa (Fig. 3a). As already recalled in Part I, values at a single gridpoint are not independent, so local t-tests are not definitive. However, since the Control precipitation is almost zero over northern Africa, the departure (RCP − Control) is significant, even if there are other regions (i.e., the Indian Ocean) where the (RCP − Control) increase is higher. The percentage (RCP − Control) departure from Control is shown in Fig. 3b. Over northern and eastern Africa, the RCP JAS precipitation at least doubles as a consequence of the changed vegetation.

In Fig. 4, the Control and (RCP − Control) JAS precipitation are displayed as in Fig. 2, but focused over northern Africa, the Middle East and the Mediterranean. There is a large northward shift of the ITCZ. Particularly, in the Control run the isohyet of 0.25 mm day^{-1} reaches the latitude of 18° North over Sudan, whereas the departure (RCP − Control) line of 0.25 mm day^{-1} goes 3° more to the north. The upper Nile Valley countries, which correspond to the ancient Nubian, Meroe and Ethiopian cultures, show an increase in rainfall, which is in agreement with the historical records of better conditions for agriculture. Overall, since the entire runoff of all northeastern Africa contributes to the Nile watershed, it appears that, with the RCP conditions, the runoff of the entire Nile watershed would be enhanced. In fact, since the Nile has its source close to the Equator, the Upper Nile crosses most of the areas subjected to the precipitation increase in the experiment.

The JAS (RCP − Control) map displays another area with an increase consistent with the historical record: the Atlas range (northwestern Africa). The relatively poor resolution of the RD experiment did not have any mountain range over northwestern Africa, and the orography plays a major role in such a well localized response in the precipitation, which borders the Algerian and Tunisian mountains.

In Europe, the high resolution RCP experiment provides a smaller and different response. The Iberian peninsula displays a positive (RCP − Control) departure (increase in precipitation), as does the area south of the Caucasus mountains (ancient Armenia) and the area immediately to the north of the Black Sea, whereas over the central–western Mediterranean the (RCP − Control) precipitation is negative. Overall, the positive–negative pattern between the Atlas range and the central Mediterranean is indicative of a stationary wave pattern. In agreement with the R15 experiment, the maximum response to the vegetation change occurs in August. In Fig. 5, in fact, all the features seen in the JAS map are confirmed: the

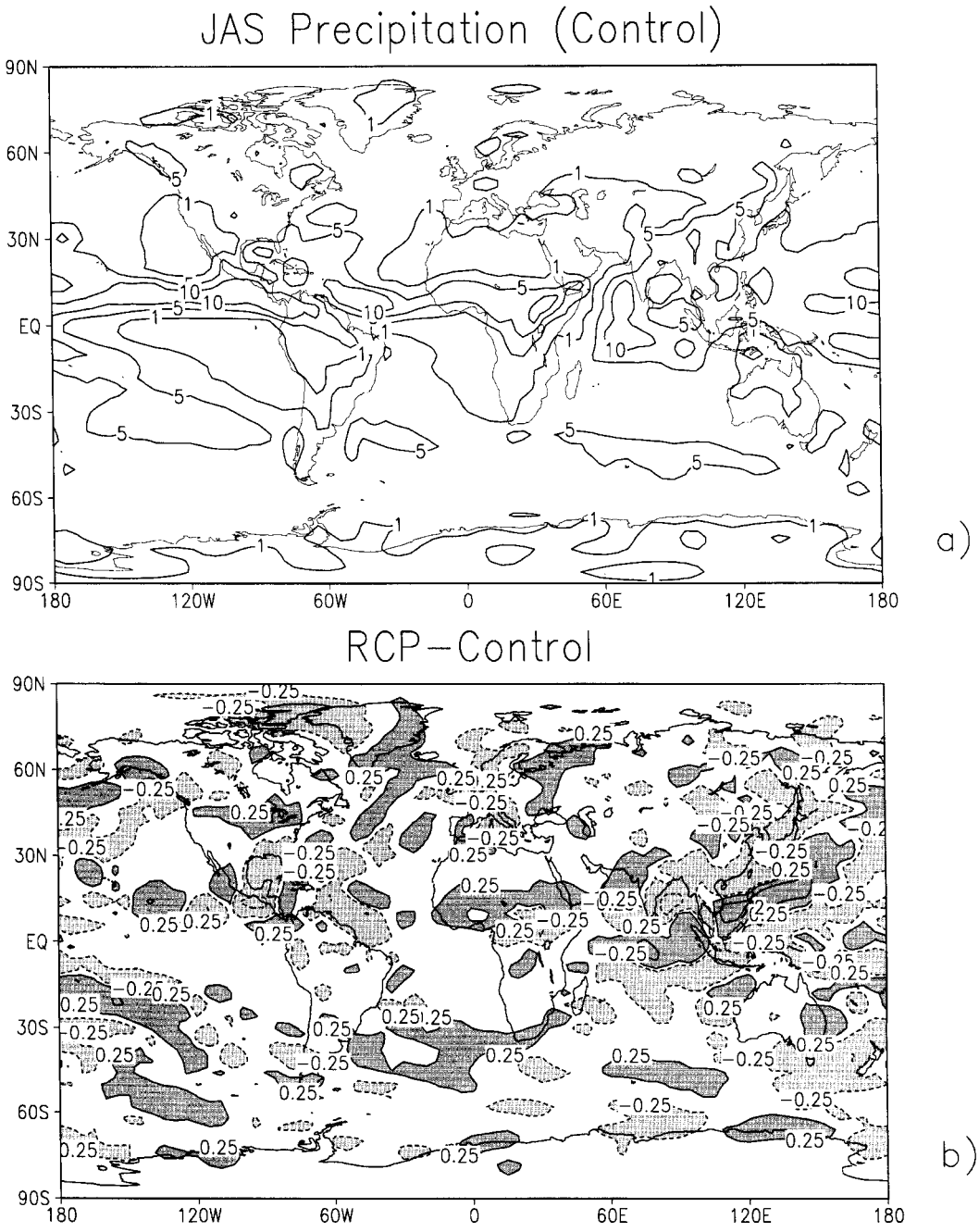

Fig. 2. Mean JAS Precipitation. Control (panel a), RCP − Control (panel b). Contours at 1, 5 and 10 mm day^{-1} in panel a and at ±2 mm day^{-1} in panel b, where the contours ±0.25 mm day^{-1} were added. It is necessary to use different contour intervals to represent the entire range of the precipitation field and the sharp gradients from the very high values in the ITCZ to the extremely small values of the Sahara. In the darker (lighter) shaded areas the RCP − Control precipitation is greater (less) than ±0.25 mm day^{-1}.

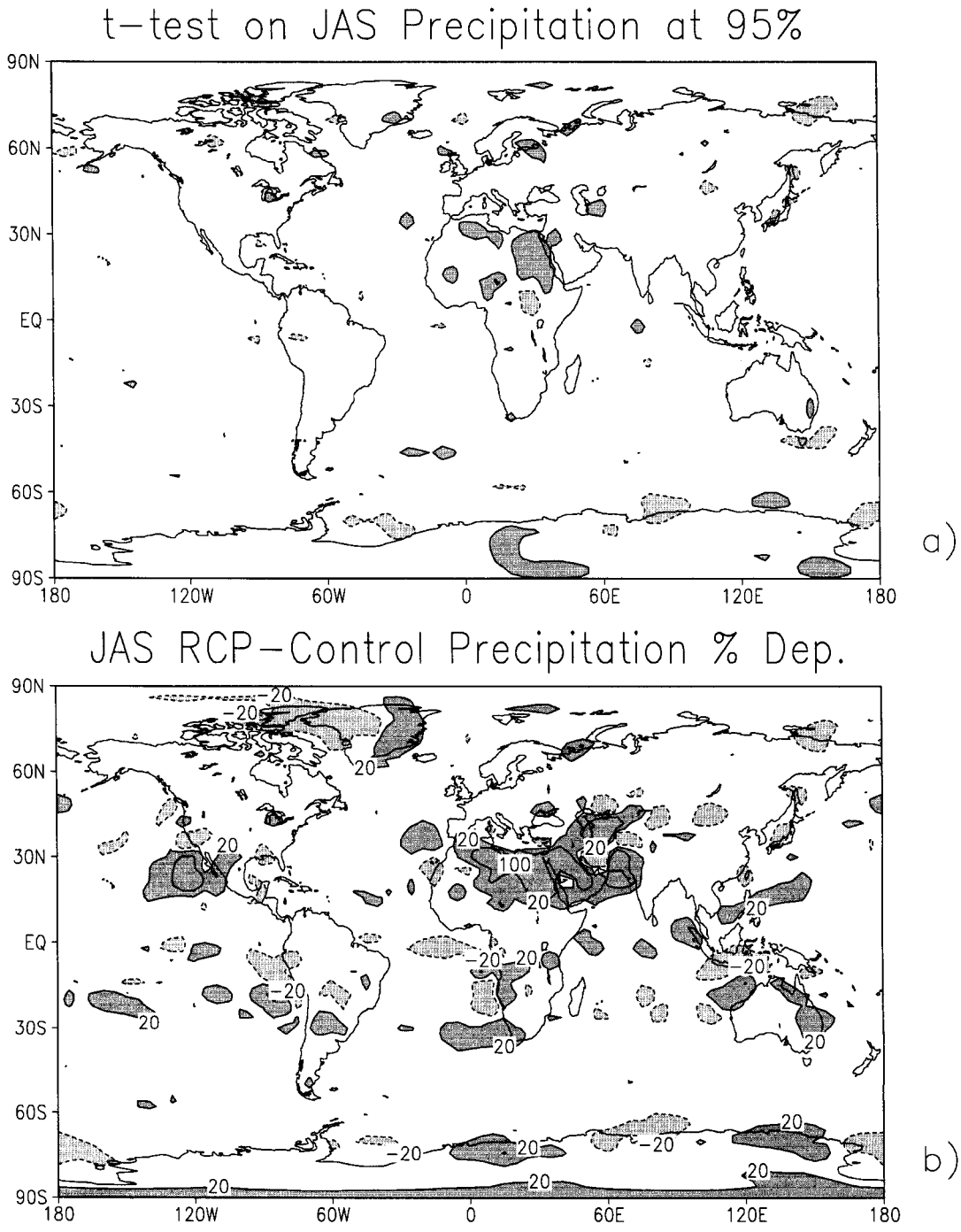

Fig. 3. *t*-Test (panel a) and percentage departure (panel b) on mean JAS precipitation. Above, in the darker (lighter) shaded areas the precipitation RCP − Control is greater (less) than zero at 5% significance. Below, contours every 100%. The contours ±20% were added. In the darker (lighter) shaded areas the RCP − Control percentage departure from Control is greater (less) than ±20%.

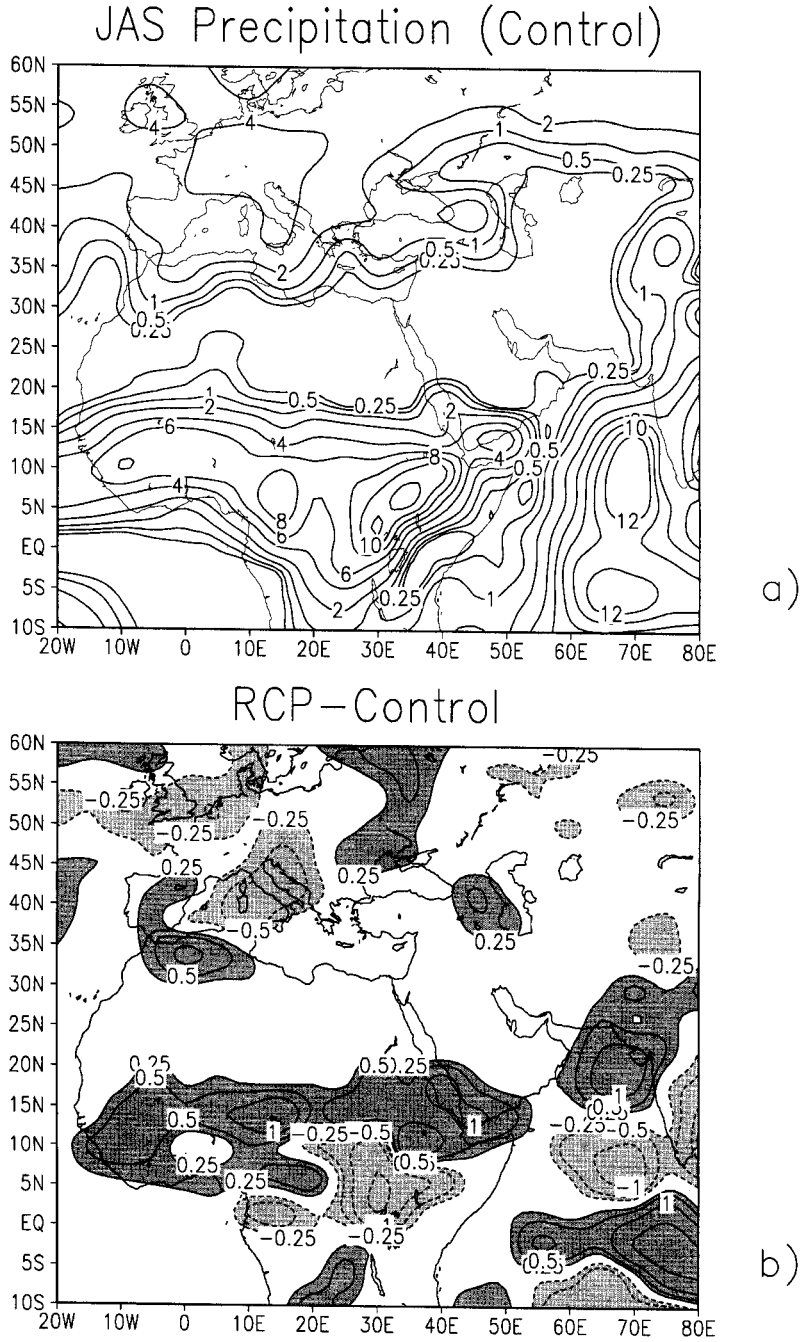

Fig. 4. Regional view of mean JAS Precipitation. Control (panel a), RCP − Control (panel b). In panel a, the contour interval is 2 mm day^{-1} (for $p_{\text{Control}} > 2$ mm day^{-1}); the contours 0.25; 0.5; 1 mm day^{-1} were added. In panel b, the contour interval is 1 mm day^{-1} (for $|p_{\text{RCP0}} - p_{\text{Control}}| > 1$ mm day^{-1}); the contours ± 0.25; 0.5 mm day^{-1} were added. In the darker (lighter) shaded areas the RCP − Control precipitation is greater (less) than ± 0.25 mm day^{-1}.

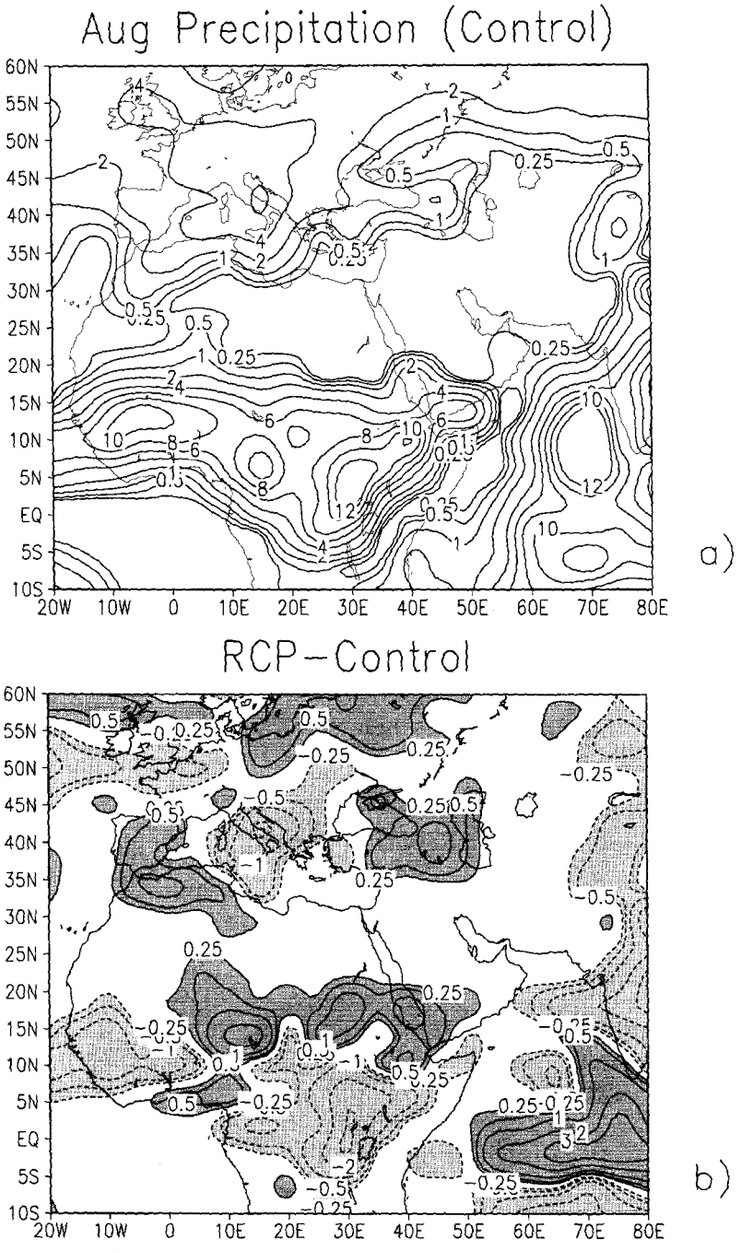

Fig. 5. August precipitation. Control (panel a), RCP − Control (panel b). In panel a, the contour interval is 2 mm day^{-1} (for $p_{Control} > 2$ mm day^{-1}); the contours 0.25, 0.5, and 1 mm day^{-1} were added. In panel b, the contour interval is 1 mm day^{-1} (for $|p_{RCP0} - p_{Control}| > 1$ mm day^{-1}); the contours ± 0.25; 0.5 mm day^{-1} were added. In the darker (lighter) shaded areas, the RCP − Control precipitation is greater (less) than ± 0.25 mm day^{-1}.

strong increase over the upper Nile Valley, as well as the positive–negative–positive pattern between western, central and eastern Mediterranean.

The time series of precipitation for the most significant areas have been calculated. The selected areas are delineated in Fig. 6 and listed geographically in Table 4. The region called Nile Valley (no. 1, from 16°N to 28°N and 27.5°E to 37.5°E) covers essentially what was named "Upper Nile" in ancient times, between the south of Roman Egypt and the areas subjected to the Kingdom of Meroe and to the Ethiopians. The Sahel (no. 2, from 12°N to 20°N and 12.5°W to 47.5°E) is a wide strip to the south of the Sahara, crossing the African continent from coast to coast. The region that is named Atlas range (no. 3, from 28°N to 36°N and 7.5°W to 12.5°E) is located in northwest Africa, including modern Tunisia and the northeast portion of Algeria and Morocco, formerly named Numidia and Mauretania. The region named Iberian Peninsula (no. 4, from 36°N to 44°N and 12.5°W to 2.5°E) corresponds to modern Spain and Portugal. Region 5 is a wide strip in the central Mediterranean area, including Italy, Greece and West Turkey, formerly Asia Minor, (from 36°N to 44°N and 2.5°E to 37.5°E). Those areas are representative of different kinds of climate changes in response to the changed vegetation. Those are the regions in which the physical and dynamical processes have been investigated.

Table 4
Areas selected for the time series of precipitation

Name of region	Latitudes	Longitudes
Nile Valley (no. 1)	16–20°N	27.5–37.5°E
Sahel (no. 2)	12–20°N	12.5°W–47.5°E
Atlas range (no. 3)	28–36°N	7.5°W–12.5°E
Iberian Peninsula (no. 4)	36–44°N	12.5°W–2.5°E
Italy, Greece and W Asia Minor (no. 5)	36–44°N	2.5–37.5°E

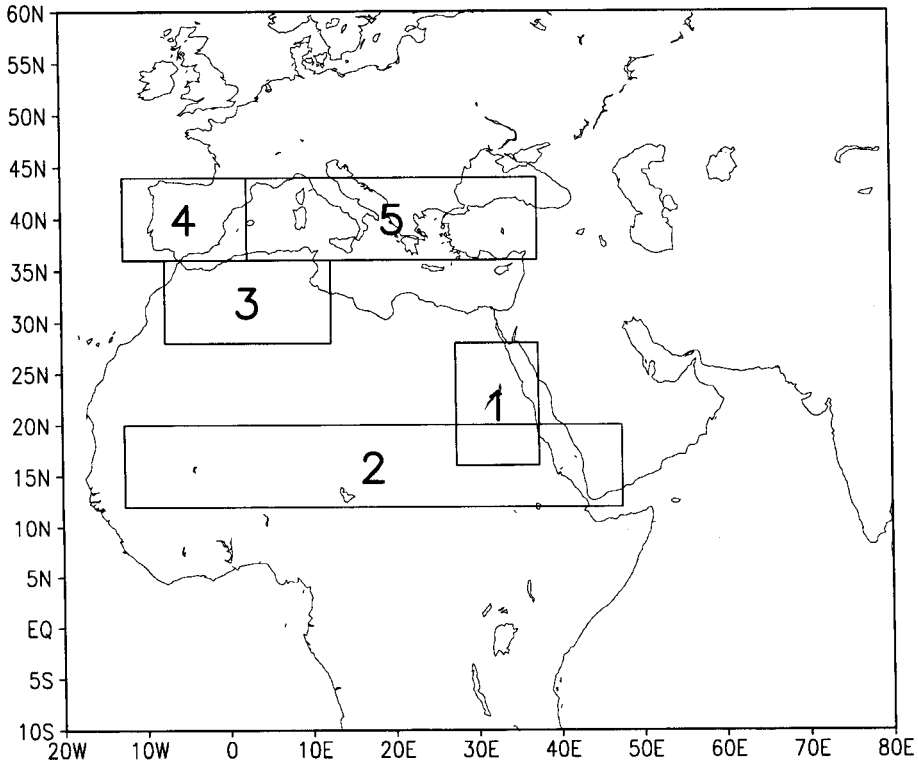

Fig. 6. Areas selected to analyze the rainfall time series and the energy budget. The latitudes and longitudes of the areas are given in Table 4. The regions are named: Nile Valley (1); Sahel (2); Atlas Range (3); Iberia (4); Central Mediterranean (5).

5.2. Ecological implications

Region 1 (Fig. 7), provides the most consistent RCP response: the (RCP − Control) time series shows that over 20 months of integration, there is no month in which the Control precipitation is greater than the RCP precipitation. The control precipitation does not reach 0.3 mm day^{-1} in any month, whereas in the RCP experiment the same threshold is reached every year in at least one month. Adding the monthly precipitation for each season, it can be seen also that over the four months JJAS, a total of 40 mm per each rainy season is reached in the RCP case but not reached in the control. This means that, in the RCP experiment, the Nile Valley experiences a shift from hyper-arid to sub-arid climate. In fact, the 0.3 mm day^{-1} precipitation, corresponding to about 9 mm month^{-1}, is generally accepted as the critical amount to distinguish between desert and subdesert environments. Furthermore, in the RCP case, the critical limit of 0.5 mm day^{-1}, usually necessary for groundcover to survive after one year of dormant life, is reached in 4 out of 5 years.

In Fig. 7 the time series for region 2, the Sahel area, is also displayed. The increase in precipitation over the Sahel in the RCP experiment is distributed over a very large area (from coast to coast across the northern African continent); the JAS average (RCP − Control) precipitation increases of 0.7 mm day^{-1} or more over an area of approximately 3 million km^2. The RCP precipitation is larger than Control precipitation 16 months out of 20, but the relevant fact, for its ecological implications, is that the 3 mm day^{-1} average over the JAS months is reached in the RCP case, and it is not reached in the Control. In fact, the RCP averaged is 3.5 mm day^{-1}, and the Control is 2.8 mm day^{-1}. 3 mm day^{-1} or 300 mm for the entire JAS season are generally accepted as the minimum requirement to support standing trees of the genus *Acacia*. The sustainability of a certain vegetational environment is a very complex subject, because plants depend on mean rainfall but much more on its variability, i.e. on extreme climatic events, and on wind, temperature, soil chemistry, soil erosion, water table response, etc. Nonetheless, the fact that the critical value of 3 mm day^{-1} is reached in the RCP run and not reached in the other, allows us to speculate that the average climate of a large area could support a savanna environment in the RCP experiment, and could not in the Control case.

The net result is that, in the RCP experiment, arid climatic conditions retreat on both their eastern and southern borders, yielding a smaller Sahara desert. It is important to note that the vegetation over the Sahel was not changed in the RCP experiment; therefore, the experiment induces a response in climate on a larger scale than the domain over which vegetation was altered.

Over region 3 (Atlas range) the time series also show a relevant increase of precipitation occurs in the RCP case, with 17 months out of 20 having a positive (RCP-Control) difference (not shown). From the environmental perspective, the change is very significant. In fact, most of the area facing the sea was covered in the RCP by Mediterranean forest, a complex environment characterized by the presence of broadleaf evergreen like *Quercus ilex*, whereas the southern flank of the eastern Atlas, currently between Tunisia and NE Algeria, was covered by savanna. The Mediterranean forest requires a very rainy winter season (which still presently occurs), but also some precipitation in the summer (about 1 mm day^{-1}, 30 mm month^{-1}), unlike Mediterranean scrub that can survive through several months of complete drought. In modern times, summer precipitation is absent over most of the southern Mediterranean. In our experiment, the critical value of 30 mm month^{-1} during the summer months is reached in the RCP case and not reached in the Control case. In fact, the average precipitation in the JAS month is 1.3 mm day^{-1} in the RCP case, and 0.9 mm day^{-1} in the Control. Including the month of June in our average, the RCP mean is 1.1 mm day^{-1}, and the Control is 0.8 mm day^{-1}.

So, in agreement with the pollen data and the historical records, it can be speculated that condi-

Fig. 7. Time series of precipitation, averaged over region 1 (Nile Valley), between latitudes 16°N–28°N and longitudes 27.5°E–37.5°E (panels a, c, e), and over region 2 (Sahel), between latitudes 12°N–20°N and longitudes 12.5°W—47.5°E (panels b, d, f). Control (panels a, b), RCP (panels c, d), RCP − Control (panels e, f). Units in mm day^{-1}. Note the difference in scale between the left and right panels.

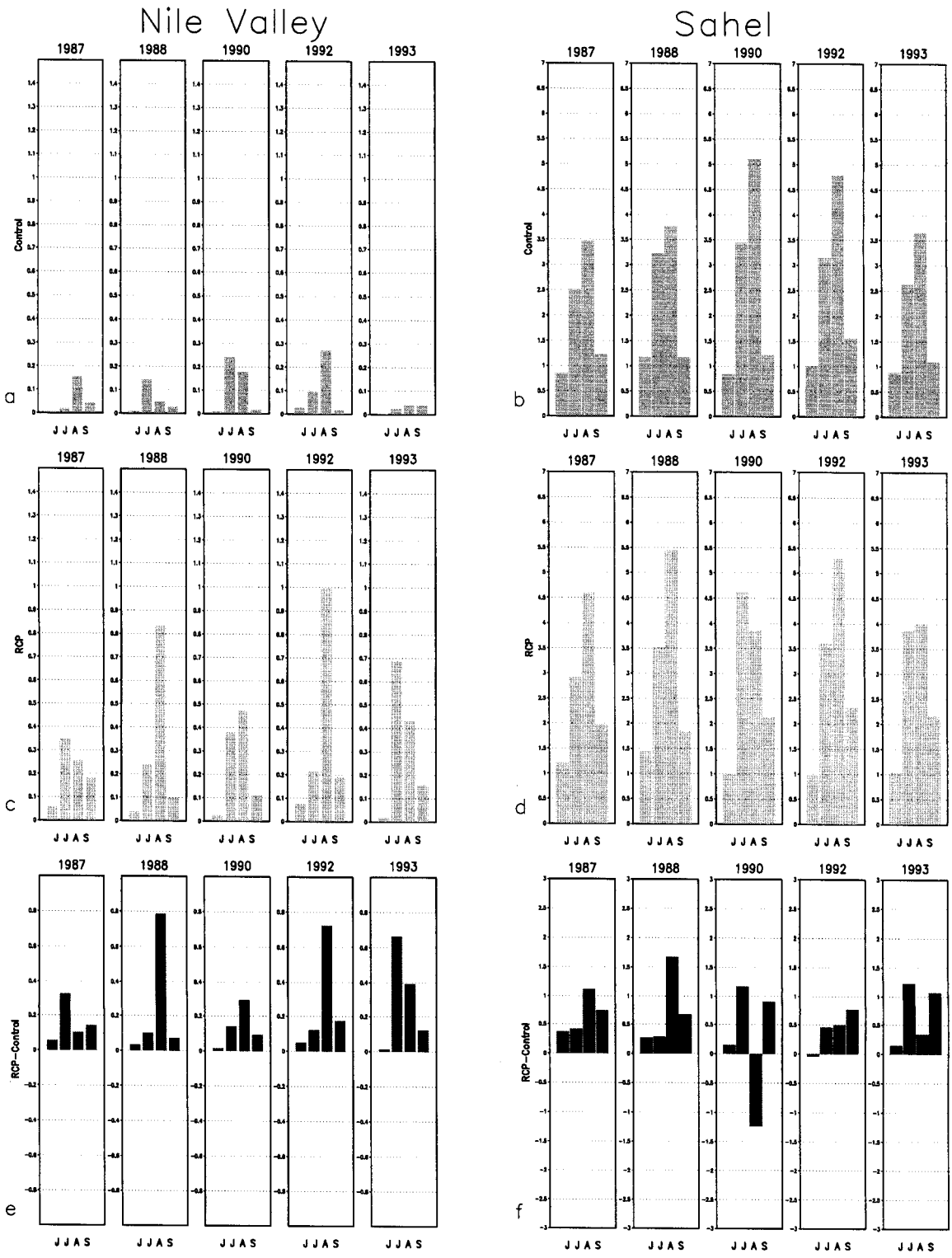
Nile Valley
Sahel
1987
1988
1990
1992
1993
Control
RCP
RCP–Control
JJAS
a
b
c
d
e
f

tions for Mediterranean forest over the northern side of the Atlas range (assuming the winter precipitation to be the same for RCP and Control, since RD did not show any signal in winter time), and savanna over the southern flank, result from the RCP experiment.

Nile Valley, Sahel and Atlas Range are the areas where the response of the RCP experiment, in terms of summer precipitation increase, is evident. The other two areas selected show more variability, perhaps due to the fact that baroclinic instability starts to be stronger with the increase in latitude.

The time series of the Iberian peninsula (region 4), reveal that the overall (RCP-Control) precipitation mean of 5 years is still positive: 4 out of 5 years display one month, either July or August, with a remarkable increase in rainfall (not shown). However, variability over this region is very high.

Region 5, namely the northern–central Mediterranean, including Italy, Greece and W Turkey (Asia Minor), is the only area affected by a negative (RCP-Control) departure, i.e., reduced rainfall in the RCP experiment. The time series displays a great deal of variability, with 9 months out of 20 having the RCP precipitation exceeding the Control, and 11 months having the opposite sign (not shown). It should be noted, however, that neither Italy nor Greece is really represented at R40 resolution; therefore, the decrease of precipitation occurs mostly over water and not over gridboxes affected by the vegetation change. The only possible way to see local effects of land surface changes over Greece and Italy would be through mesoscale modeling.

5.3. Evaporation and temperature

The JAS Control evaporation field, averaged over the 5 years of integration, together with the departure (RCP – Control), is presented in Fig. 8. The control evaporation field displays a very large area with values less than 1 mm day^{-1}, from the Sahara desert to central Asia. Three areas of positive (RCP – Control) departures are present over the Sahel, the Atlas range and the Middle East. Of these, the first two are 95% significant.

In Fig. 9, the JAS precipitation minus evaporation fields are displayed over our region of interest. The Control precipitation minus evaporation fields are positive slightly to the north of Equatorial Africa, related with the ITCZ position, and negative over the entire Mediterranean, which is known to be a sea where evaporation exceeds precipitation in summer. The (RCP – Control) departures display a strong increase over the Sahel and the Nile Valley, an increase over the Atlas range and the Iberian Peninsula, a decrease over most of the central Mediterranean. The implications of these pictures, in terms of vegetational environments, are noteworthy. The Sahelian, Nile and Atlas regions drift, in the RCP experiment, toward a significantly moister climate, and, to a lesser extent, the Iberian Peninsula and Armenia do the same. On the other hand, the central Mediterranean experiences moisture flux divergence.

Fig. 10 shows the JAS Control surface temperature averaged over the 5 years of integration, together with the corresponding (RCP – Control) departure. A large increase in temperature occurs over much of northern and northeastern Africa and the Arabic peninsula, including central Sahara (where the vegetation was not changed). The warm anomaly originated by the change in vegetation over northern Africa is advected towards the Sahara by the low-level northeasterly flow, as will be discussed in the next sections. The anomaly can also be seen aloft: it reaches the upper branch of the Hadley circulation and then, at 700 hPa, is spread and advected northeastward, crossing the entire Asian continent (not shown). The temperature anomaly across levels can be tracked up to 300 hPa. This feature was also observed in the RD experiment.

5.4. Surface heat budget

The varied response in the precipitation field suggests a separate analysis over the 5 selected areas (seen in Fig. 6) that were already chosen to display the rainfall time series. The surface energy budget under steady conditions is defined as

$$SW\Downarrow + SW\Uparrow + SH + LH + NLW = G \qquad (1)$$

where SW $\Downarrow$ is the downgoing short wave, SW $\Uparrow$ is the upgoing short wave, SH is the sensible heat, LH is the latent heat, NLW is the net long wave and G is the heat flux into the ground surface, calculated as a residual. Over the entire year, G is normally zero,

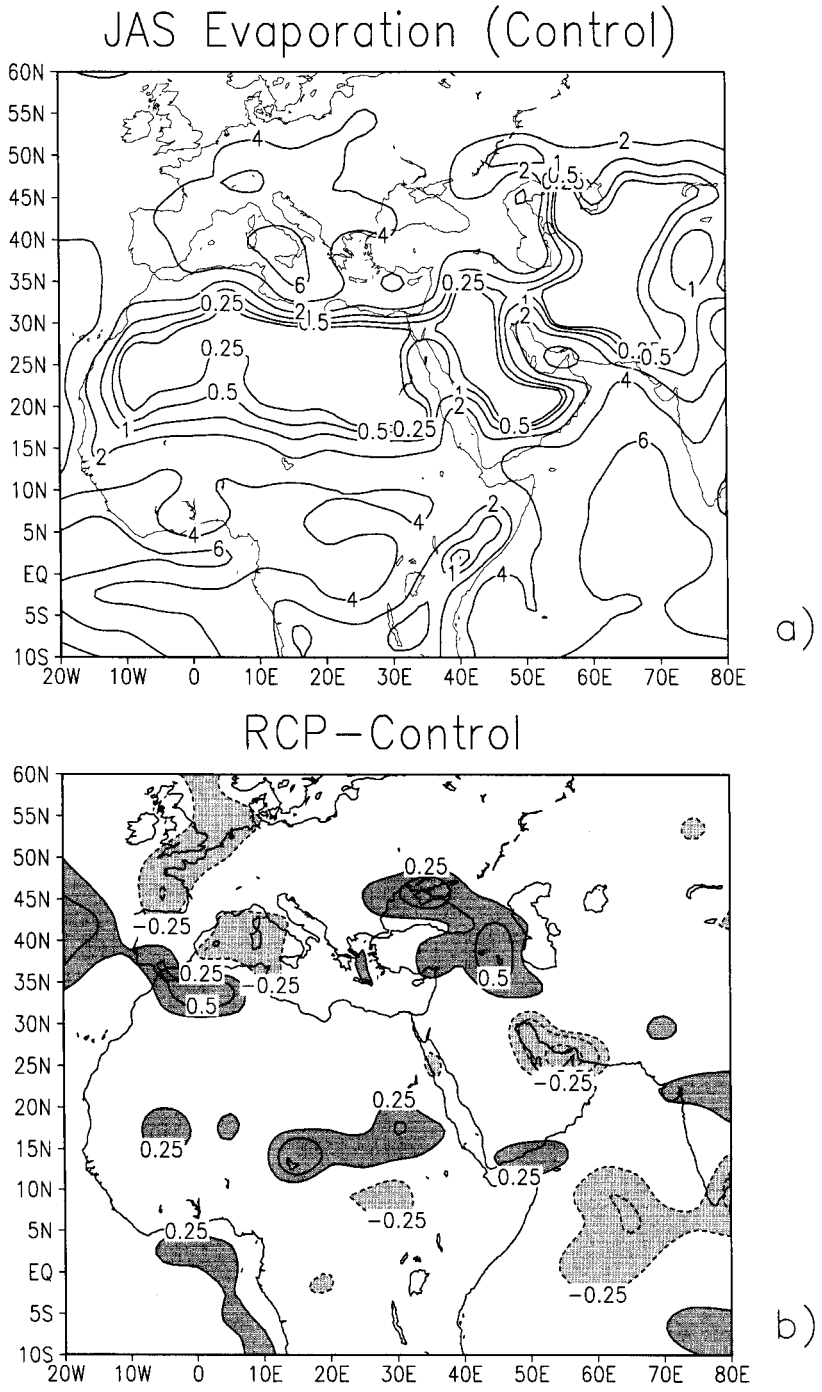

Fig. 8. Regional view of JAS evaporation. Control (panel a), RCP − Control (panel b). In panel a, the contour interval is 2 mm day^{-1} (for $e_{\text{Control}} > 2$ mm day^{-1}); the contours 0.25; 0.5; 1 mm day^{-1} were added. In panel b, the contour interval is 1 mm day^{-1} (for $|e_{\text{RCP0}} - e_{\text{Control}}| > 1$ mm day^{-1}); the contours ± 0.25 and 0.5 mm day^{-1} were added.

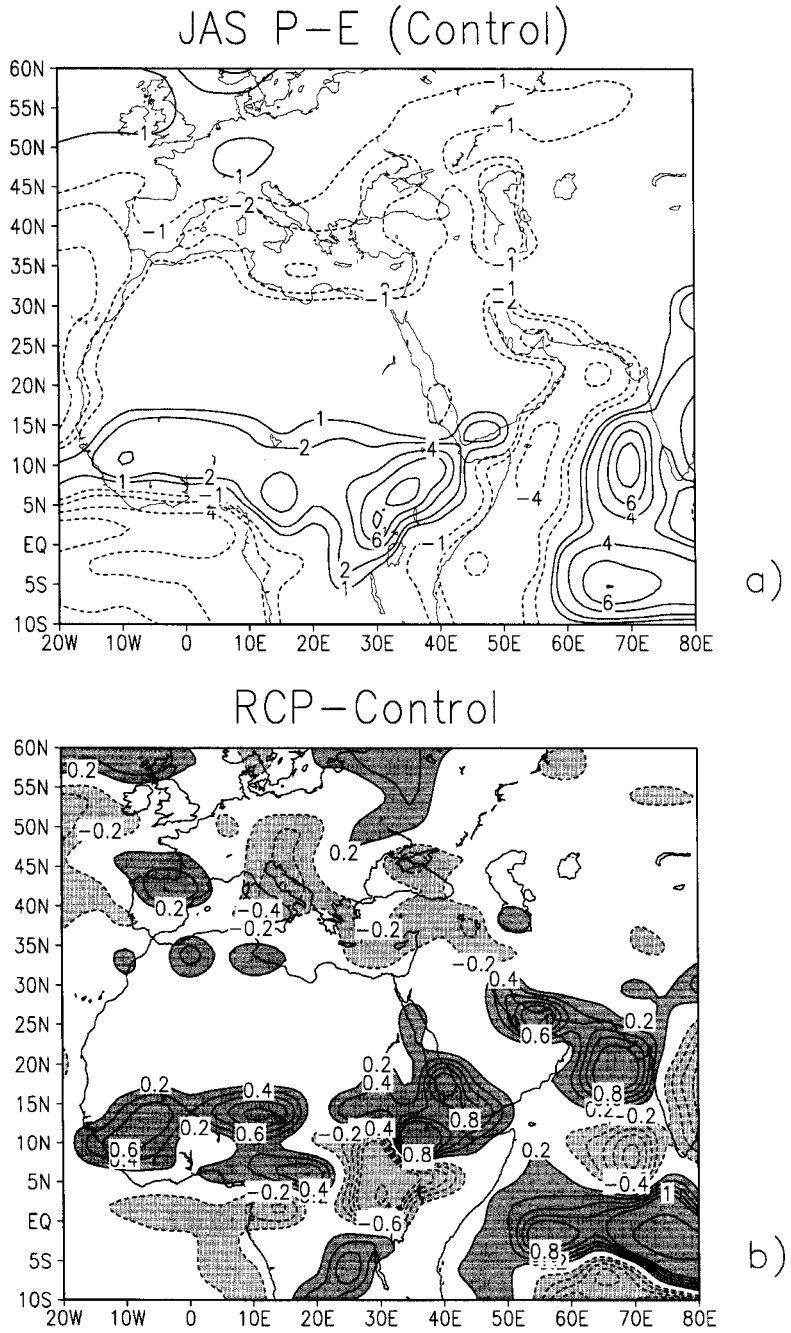

Fig. 9. Regional view of JAS precipitation–evaporation. Control (panel a), RCP − Control (panel b). In panel a, the contour interval is 2 mm day^{-1}. The zero is not plotted, and the contours ± 1 mm day^{-1} were added. In panel b, the contour interval is 1 mm day^{-1} (for $|(p-e)_{\mathrm{RCP}}-(p-e)_{\mathrm{Con}}|>1$ mm day^{-1}) and 0.2 mm day^{-1} (for $|(p-e)_{\mathrm{RCP}}-(p-e)_{\mathrm{Con}}|<1$ mm day^{-1}). In the darker (lighter) shaded areas the $(p-e)_{\mathrm{RCP}}-(p-e)_{\mathrm{Con}}$ is greater (less) than ± 0.2 mm day^{-1}.

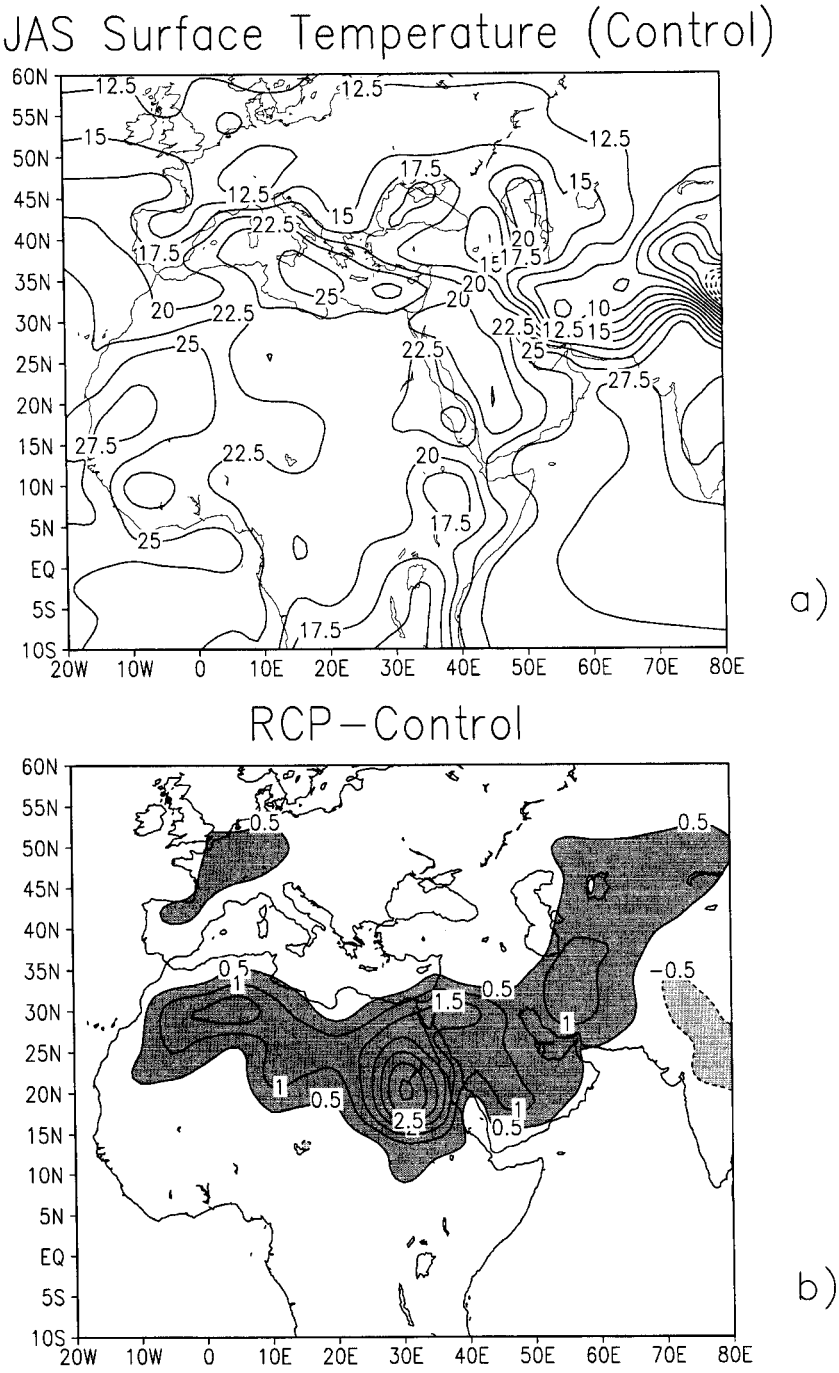

Fig. 10. Regional view of JAS surface temperature (i.e., top soil layer skin temperature). Control (panel a), RCP – Control (panel b). In panel a, the contour interval is 2.5°C. In panel b, the contour interval is 0.5°C. In the darker (lighter) shaded areas the RCP – Control surface temperature is greater (less) than ±0.5°C.

but can be nonzero over seasonal period: it represents a subsurface sensible flux or a storage term. Since our concern is to explain the surface temperature increase in terms of fluxes towards and from the ground surface, downward quantities are regarded as positive whereas upward fluxes are negative.

The areas chosen to calculate the surface energy budget are the same used to describe the precipitation field (Fig. 5 and Table 4), although another region, namely "Sahara", from 20°N to 32°N and 7.5°W to 37.5°E, is included, to better understand the large increase in temperature observed in Fig. 10.

Beginning from this area, it can be seen that in the surface balance displayed in Table 5 there is a decrease in downward short wave radiation because of the increased cloudiness in the RCP case but a larger decrease in the upward short wave radiation because of the decreased albedo (the northern and eastern parts of the area have a vegetation change). Overall, there is a net short wave increase of 12 W m^{-2}. The area also displays a substantial increase of sensible heat (13 W m^{-2}) in the RCP case, caused by the increased temperature, a small increase in latent heat of 1 W m^{-2}, and a decrease in net long wave radiation, due to the increased cloudiness. The residual term has a positive (RCP − Control) departure of 1 W m^{-2} that justifies the warmer RCP temperature. It is interesting that warmer temperatures with lower albedo seem in apparent contradiction with the results found by Nobre et al. (1991), by Dirmeyer (1992) or by Dirmeyer and Shukla (1994). In these studies, the authors found a temperature increase over the Amazon as a consequence of the deforestation, with increased albedo. The reason for this different response is that in a tropical forest a large fraction of the decreased upward short wave radiation due to darker vegetation (i.e., lower albedo) becomes energy available for evaporation if the ground is saturated or very moist. In a sub-desert environment, the net increase of solar radiation due to lower albedo is the dominant part of the surface energy budget. The increased flux of latent heat, related to increases of precipitation and soil moisture, cannot balance the increase in short wave radiation. Our result is consistent with previous experimental (Otterman, 1989; Otterman and Tucker, 1985) and modeling results (Otterman, 1992). Particularly, in the latter study the author modeled the effects of desert-scrub growth as a forcing towards a "warmer and more pluvial climate".

Table 5
Mean JAS surface energy budget (Sahara). Values in W m^{-2}

Sahara	SW ⇓	SW ⇑	Net SW	SH	LH	Net LW	G
Z1	344	101	243	97	8	135	2
RCP1	337	82	255	110	9	132	3
RCP1-Z1	−7	−19	12	13	1	−3	1

Table 6
Mean JAS surface energy budget over five areas. Values in W m^{-2}.

	SW ⇓	SW ⇑	Net SW	SH	LH	Net LW	G
Nile							
Z1	349	95	254	92	10	143	8
RCP1	332	60	272	115	13	133	11
RCP1-Z1	−17	−35	18	23	3	−10	3
Sahel							
Z1	295	69	226	74	53	99	0
RCP1	282	64	218	70	61	88	−1
RCP1-Z1	−13	−5	−8	−4	8	−11	−1
Atlas							
Z1	317	78	239	88	35	110	6
RCP1	303	51	252	101	42	101	7
RCP1-Z1	−14	−27	13	13	7	−9	1
Iberia							
Z1	280	33	247	30	111	70	36
RCP1	271	24	247	28	112	66	41
RCP1-Z1	−9	−9	0	−2	1	−4	5
C. Med.							
Z1	275	25	250	26	133	75	16
RCP1	276	21	255	26	132	76	21
RCP1-Z1	1	−4	5	0	−1	1	5

Table 6 gives the surface energy budget for the five areas listed in Table 4 and shown in Fig. 6. The Nile region (no. 1) shows a net increase in the storage term of 3 W m^{-2} as a consequence of the RCP experiment, in agreement with the strong increase in surface temperature (Fig. 10). As seen for the Sahara region, the downward short wave radiation decreases in the RCP experiment because of the increased cloudiness, but the upward short wave radiation also decreases because of the decreased albedo, the former effect prevailing over the latter. As a result, the net short wave is substantially increased over the Nile Valley by 18 W m^{-2}. As a consequence of warmer temperatures and of increased turbulent heat transfer efficiency between

ground and air, triggered by higher roughness, sensible heat increases too. Latent heat is also increased because of the increased rainfall, but the net long wave radiation is reduced because of the increased average cloudiness. Again, the variations of fluxes and the increase of temperature consequent to the decrease in albedo are consistent with Otterman (1992), which shows how scrubs into a desert environment force climate towards higher temperatures and increased rainfall.

It can be seen from Figs. 4 and 10 that the maximum increase in precipitation, over the Sahel, occurs to the south of the area with the maximum increase in surface temperature, which corresponds mostly to the Sahara desert. This is reflected in the heat budget for region 2. In fact, the increase in cloudiness and precipitation occurring over the Sahel reduces both downward and upward short wave at the surface. The net short wave radiation decreases by 8 W m^{-2}, which means that the reduction in downward short wave due to cloudiness is predominant. Sensible heat and net long wave both decrease, whereas latent heat increases, coherently with the increased precipitation. The total (RCP-Control) energy residual is less than -1 W m^{-2}: a very small fraction ($< 1/100$) of the terms involved in the budget.

The heat budget of region 3 (Atlas) shows that, for the short wave radiation, the effect of decreased upward flux due to lower albedo is larger than the reduction of downward flux due to increased cloudiness, so that the net short wave is increased by 13 W m^{-2}. Sensible heat and latent heat increase and net long wave decreases. Region 4 (Iberian Peninsula), although with much smaller values, has (RCP − Control) variations with the same sign as those of the Sahel budget, but with one difference: there is no change in the net short wave radiation. This is due to the fact that the decreased upward short wave due to the decreased albedo is exactly balanced by the decreased downward short wave associated with increased cloudiness. Since the downward and upward short wave was assumed to have opposite sign, this explains the lack of variation in the net short wave.

Region 5 (central Mediterranean) displays a decrease in upward short wave, consistent with the lower albedo, but a larger increase in downward short wave due to decreased cloudiness: therefore the net short wave increases of 5 W m^{-2}. There is a small decrease in latent heat by -1 W m^{-2} due to a small decrease in precipitation and a 1 W m^{-2} increase in net long wave. However, given that the departures are small, the net storage (RCP − Control) term is quite large (5 W m^{-2}), but it cannot be converted into surface temperature increases because most of the area is covered by water, and the sea surface temperature in the Control and RCP runs is the same.

5.5. Wind field, divergence and moisture flux divergence

The atmospheric circulation is altered as a consequence of the RCP vegetation. The JAS 850 hPa wind flow, which is the lowest level that does not intersect land over most of Africa in the R40 topography, reveals a northward shift of the RCP ITCZ over eastern Sahel, especially over Sudan, and over western Sahel too, whereas no significant change occurs over most of central Sahel (not shown). The ITCZ shift is very evident in the meridional cross-sections of moisture flux divergence, as will be shown later.

Fig. 11 shows the 300 hPa wind. A ridging tendency appears over the central Mediterranean in the (RCP − Control) circulation, together with a northerly (RCP − Control) component over central Sahara. In Fig. 12, where the Control JAS sea level pressure and its (RCP − Control) is displayed, it is possible to see that most of the area of interest for the present study is subjected to a pressure decrease in the RCP experiment, except the central Mediterranean, corresponding to the ridging tendency in the 300 hPa wind. The 300 hPa divergence field reveals positive values over the areas affected by an increase of precipitation (not shown).

The JAS divergence profiles averaged over the region no. 1 (Nile Valley) are displayed in Fig. 13a. The Control profile shows divergence from 850 up to 500 hPa, and convergence above that level. The RCP profile shows a surprising inversion of the pattern: there is convergence instead of divergence at 850 hPa. From the 700 hPa level and above, the (RCP − Control) profile is divergent. Over region 2, the Sahel, the profile is similar (not shown): strong convergence at 850 hPa in the control, and diver-

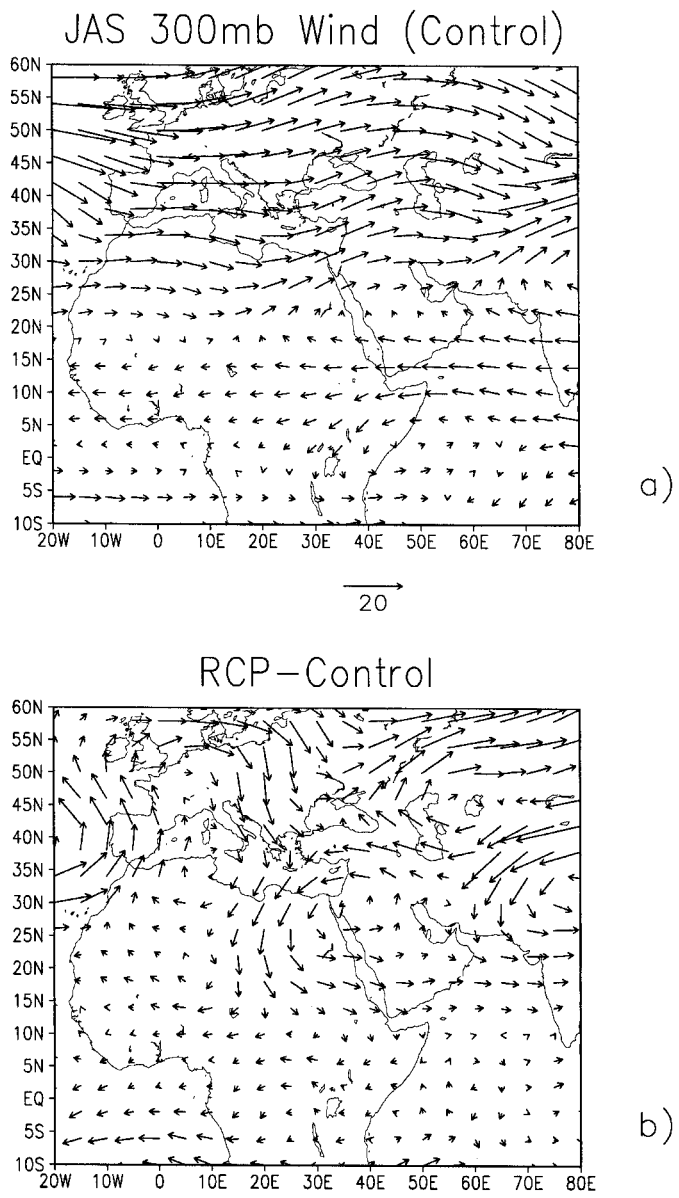

Fig. 11. JAS wind at 300 hPa. Control (panel a), RCP (panel b) and RCP − Control (panel c). In panel a, the vector scale in 20 m s^{-1}. In panel b, the vector scale in 4 m s^{-1}.

gence at 700 hPa and above. The (RCP − Control) over the Sahel does not have any change at the lowest level, but has negative values at 700 hPa. The overall result for the RCP case is a decrease of divergence at 700 hPa and an increase of divergence at 300 and 200 hPa. This is a clear indication of deeper overturning of the atmosphere, with more favorable conditions for deep convection instead of shallow convection to occur.

Divergence maps at various levels suggest the idea of a stationary wave, induced by the RCP vegetation, with consequent circulation between the Mediterranean and the Atlas region: upper level convergence over the central Mediterranean and sea

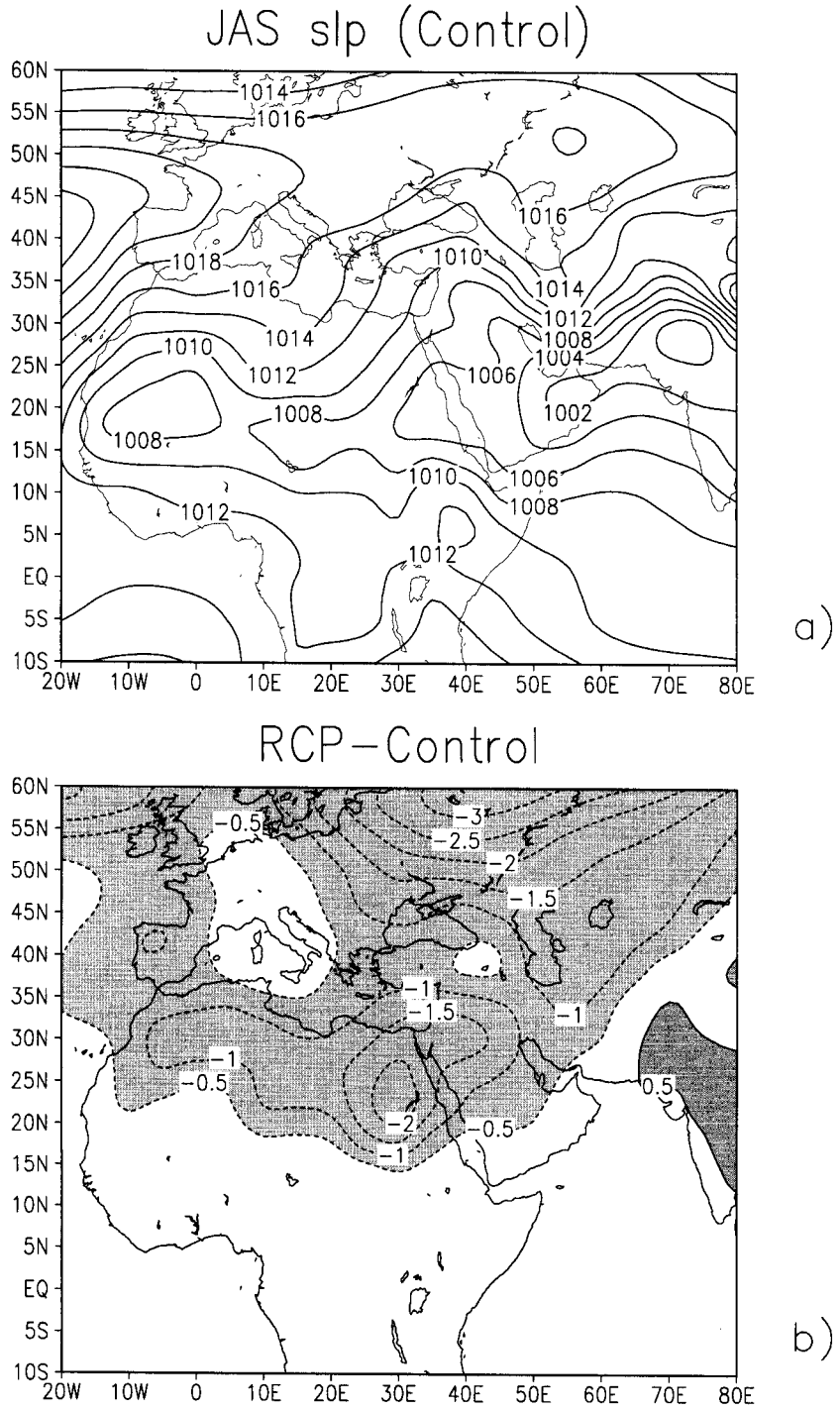

Fig. 12. Mean JAS sea level pressure. Control (panel a), RCP − Control (panel b). In panel a, the contour interval is 2 hPa. In panel b, the contour interval is 0.5 hPa. In the darker (lighter) shaded areas $slp_{RCP} - slp_{Control}$ is greater (less) than ±0.5 hPa.

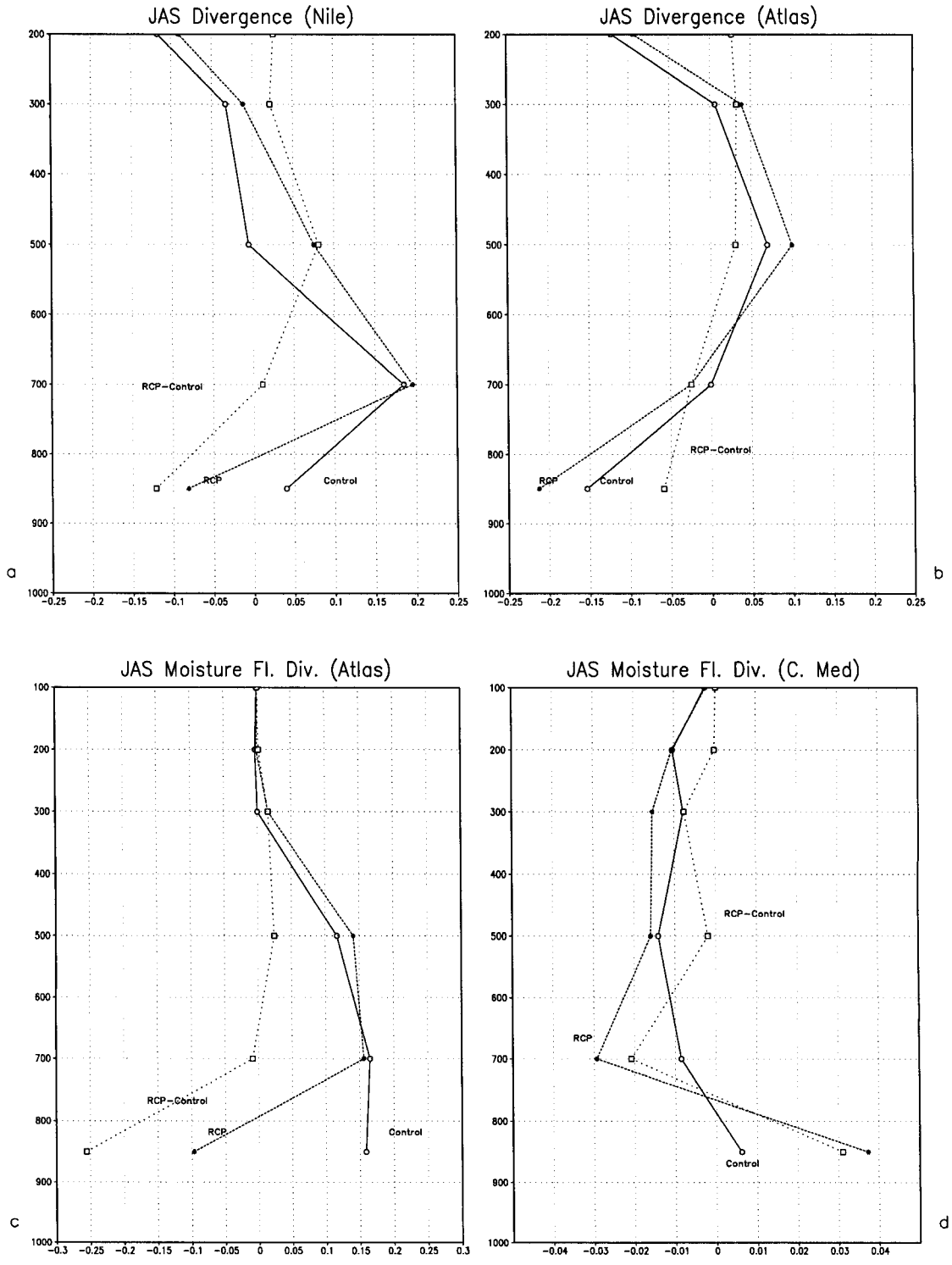
JAS Divergence (Nile)
JAS Divergence (Atlas)
JAS Moisture Fl. Div. (Atlas)
JAS Moisture Fl. Div. (C. Med)
RCP–Control
RCP
Control
a
b
c
d

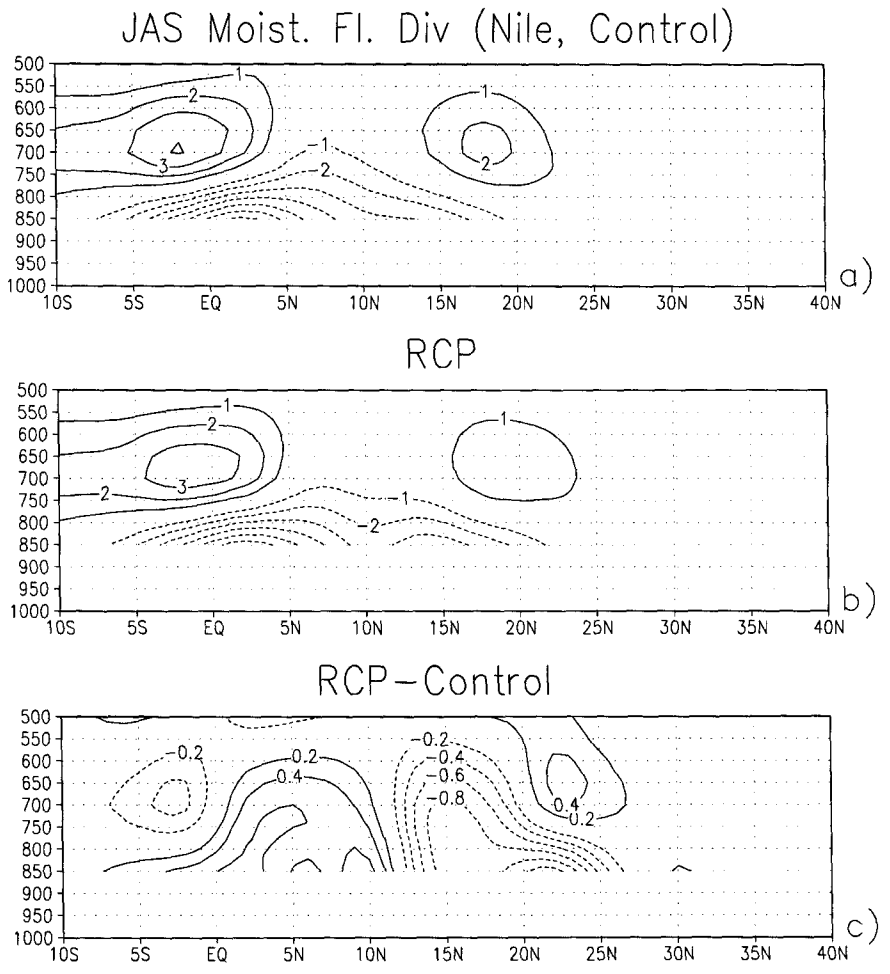

Fig. 14. JAS meridional cross-section of moisture flux divergence averaged over the longitudes of region 1 (Nile). Control (panel a), RCP (panel b), RCP – Control (panel c). Values in 10^{-8} kg m^{-3} s^{-1}. Vertical coordinate in hPa.

level pressure falling with increase of low level convergence over the Atlas range. The profile for the Atlas range (Fig. 13b) supports this idea: the 850 hPa Control convergence is increased by about 30% in the RCP case. The 700 hPa level, which is non-divergent in the Control case, becomes convergent in the RCP case, but the 500 hPa level, which is divergent in the Control case, gets an increase in divergence of about 50% in the RCP case. Overall, the three areas (Nile, Sahel and Atlas) have an RCP increase in low level convergence and upper level divergence, consistent with the increase in precipitation. The opposite pattern occurs over the central Mediterranean (not shown), as expected, since the precipitation there decreases. The RCP case shows a decrease in low level convergence (by 30% at 850

Fig. 13. Mean JAS vertical divergence profile averaged over region 1 (Nile Valley, panel a) and over region 3 (Atlas Range, panel b). Control (solid line), RCP (dashed line), RCP – Control (dotted line). Values in 10^{-5} s^{-1}. Vertical coordinate in hPa. Mean JAS vertical moisture flux divergence profile averaged over region 3 (Atlas range, panel c) and over region 4 (Central Mediterranean, panel d). Control (solid line), RCP (dashed line) and RCP – Control (dotted line). Values in 10^{-8} kg m^{-3} s^{-1}. Vertical coordinate in hPa.

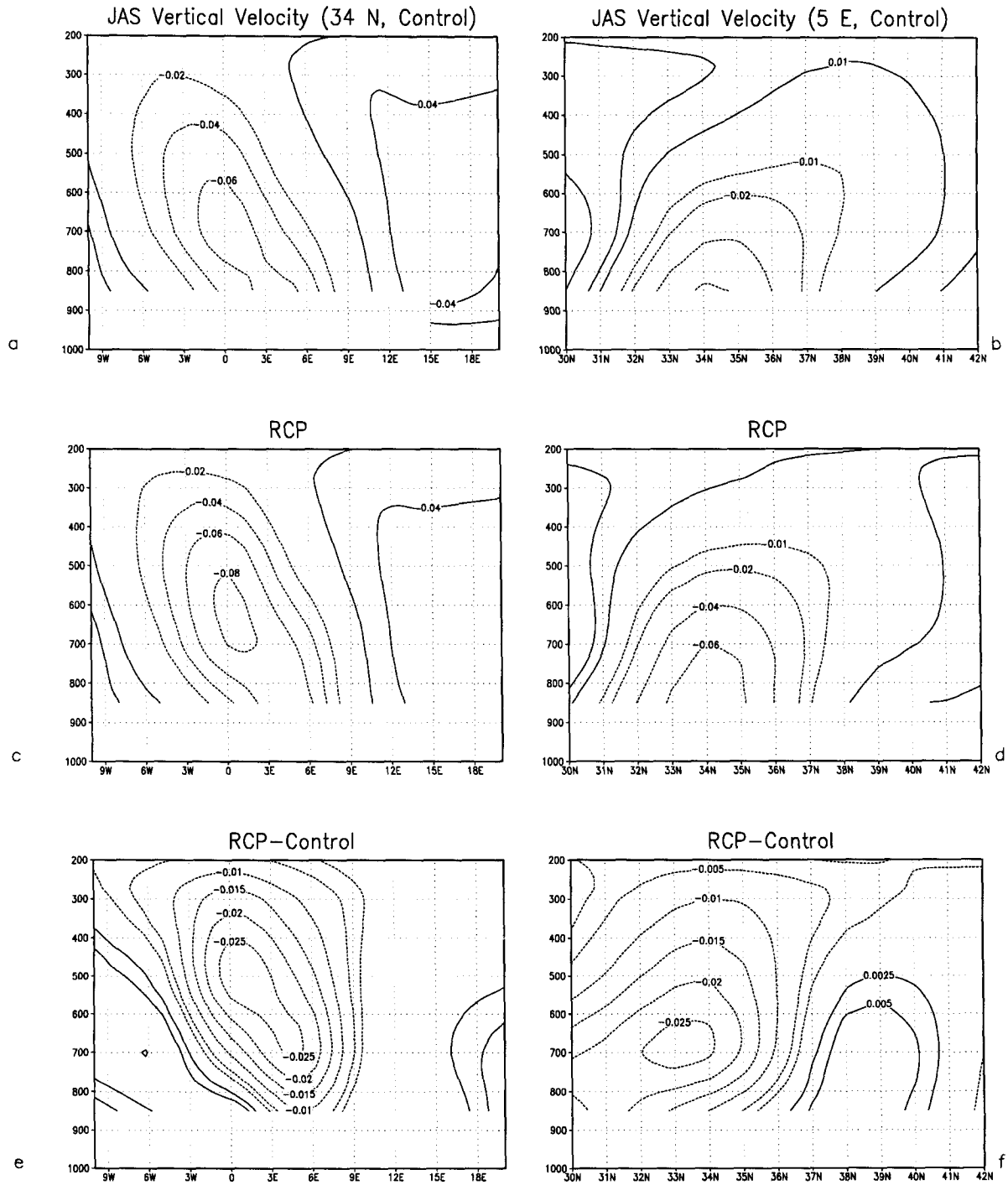

Fig. 15. JAS cross-section of omega at 34°N (panels a, c, e) and at 5°E (panels b, d, f). Control (panels a, b), RCP (panels c, d) and RCP − Control (panels e, f). Values in 10^{-3} hPa s^{-1}. Vertical coordinate in hPa.

hPa). At 300 hPa, where the Control case displays almost zero divergence, the RCP case is strongly convergent.

In Fig. 14, a meridional cross-section of moisture flux divergence $\nabla \cdot (q\mathbf{V})$ (where q is the specific humidity in kg m^{-3} and $\mathbf{V}$ is the horizontal wind in m s^{-1}), averaged between 27.5°E and 37.5°E, i.e., a strip wide as region 1, shows a well defined dipole in the (RCP − Control) case, with an indication of a northward shift of the ITCZ. Particularly, it can be seen that the $-1 \times (10^{-8})$ kg m^{-3} s^{-1} line intersects the 850 hPa level at about 19°N in the Control case and at about 22°N in the RCP case. The same dipolar pattern, although weaker, can be seen on a meridional cross section (not shown) averaged between 12.5°W and 47.5°E (from coast to coast across northern Africa, thus including regions 1 and 2). Thus, the Nile Valley and the Sahel are both responding to the same mechanism: the Nile Valley can be thought as the extreme Eastern section of the Sahel in which the ITCZ response is the most statistically significant.

The Atlas range responds to a different mechanism, not related to the ITCZ. The vertical profiles of moisture flux divergence averaged over regions 4 (Atlas) and 5 (central Mediterranean) are shown in Fig. 13c and d. Over the Atlas, the Control profile is divergent at all levels. The (RCP − Control) profile is strongly convergent at 850 hPa (-0.25×10^{-8} kg m^{-3} s^{-1}) compared with the Control value (0.17×10^{-8} kg m^{-3} s^{-1}) so that the RCP profile becomes convergent instead of divergent. This is a major change in the dynamics over the Mediterranean region, and is linked with the opposite pattern detected over region 5 (Fig. 13d), where the low-level moisture flux divergence is enhanced in the RCP case.

Any meridional cross section, across the longitudes of region 3 (7.5°W to 12.5°E), shows a negative (RCP − Control) departure (i.e., more moisture flux convergence) corresponding to the Atlas range (between 30°N and 36°N), and a positive (RCP-Control) departure corresponding to the western Mediterranean.

The dipole pattern found in the precipitation, evaporation, precipitation minus evaporation, sea level pressure and divergence profiles between the Atlas range and the central Mediterranean indicates that, in the RCP experiment, the Central Mediterranean acts as a divergent source of moisture flux, whereas the Atlas range acts as a convergent sink of moisture flux. In fact, zonal and meridional cross sections of the vertical velocity (Fig. 15) display a coupled circulation between the Atlas range and the central Mediterranean. In the zonal section (at 34°N) the rising motion is maximum at longitude 0°, and sinking motion takes place over the central Mediterranean. The meridional cross-section (longitude 5°E) displays upward motion, enhanced in the RCP experiment, between 30° and 36°N (over the Atlas range), and sinking motion between 37° and 40°N (over sea). The circulation is similar to a small scale "monsoon": the Mediterranean sea experiences upper level convergence, sinking motion and low level moisture divergence, and the Atlas range the opposite.

Streamlines of the zonal and meridional flow confirm a circulation enhanced by the RCP experiment, explaining the increase in precipitation occurring over the Atlas range. In the RCP case, the northerly component of the 850 hPa flow is reduced, and the easterly component is enhanced from 0° to 10°E, in the center of the Atlas mountains, and shows an upward motion triggered by the RCP increase in temperature and by the orography.

6. Mechanism of the response

The decreased albedo due to the RCP vegetation generates an increase of surface temperature (Fig. 10) over most of northern Africa. The low-level flow, which is northeasterly over Africa and Arabia, advects warmer temperature towards the south. Consequently, the sea level pressure falls more than 1 mbar over the entire northern African region, on an area much larger than the one in which the vegetation was changed (Fig. 12). The sea level pressure fall occurring to the north of the ITCZ trough allows a deeper penetration of the ITCZ into the African continent and the warming of the areas to the north of the ITCZ strengthens the rising motion of the Hadley cell. The increased surface temperature could not cause by itself a relevant increase in precipitation. Convection induced by mere surface warming is generally shallow convection and takes place mostly within the boundary layer without reaching

the mid troposphere. The large precipitation increase in this experiment can be attributed to the surface warming that takes place in proximity of the ITCZ, enhancing and shifting northward the deep convection environment caused by large scale convergence.

The relatively large area of western and central Sahara in which precipitation does not increase, suggests that the mechanism of the response obtained over northwestern Africa is not related to the northward shift of the ITCZ, which is the source of moisture for the Sahelian region. The increase in precipitation over the Atlas countries (and, to a lesser extent, over the Iberian peninsula) on one side, and the decrease of precipitation over the central Mediterranean (Figs. 4 and 5) on the other, would suggest that at least some of the moisture increase over the Atlas could be caused by moisture flux diverging over the Mediterranean and converging over northwestern Africa in a stationary wave pattern.

The mechanism proposed to explain both the increase and decrease of precipitation is the following: the lower albedo due to the RCP vegetation creates an increase of temperature over all of northern Africa (Fig. 10) and the Middle East, as seen from the surface energy balance. The sea level pressure falls almost everywhere there is land (Fig. 12), except over the central Mediterranean and part of France and Germany, where the (RCP-Control) pressure change is almost zero. The southern part of this area experiencing no change in sea level pressure is almost exclusively covered by water and the Italian peninsula (almost not represented even at R40 resolution). Consequently, the RCP sea level pressure displays a diminished northerly flow over the central Mediterranean, which means less summer baroclinic activity over Italy in the RCP experiment. In fact, the northerly component of the baroclinic flow is the most important cyclogenetic feature on the lee of the Alps (Buzzi and Tibaldi, 1978; Speranza et al., 1985). The flow becomes more easterly over the central southern Mediterranean. A relatively anticyclonic (RCP − Control) circulation appears over Italy, and a relative cyclone over the Atlas range, consistent with the sea level pressure map (Fig. 12). A "ridging" tendency over the western Mediterranean is detectable even at 300 hPa (Fig. 11), where a relative (RCP − Control) anticyclonic circulation can be seen. A strong anti-correlation appears in the (RCP − Control) divergence profile over the Atlas region and the profile averaged over the central Mediterranean, suggesting the idea of a dipole between those two areas: low level convergence is increased over the Atlas range and decreased over the Mediterranean, whereas upper level divergence is increased over the Atlas range and upper level convergence is increased over the central Mediterranean. The moisture flux convergence profiles for the Atlas region (Fig. 13c) and the central Mediterranean (Fig. 13d) show again an opposite and anti-correlated pattern. Zonal and meridional cross-sections of vertical velocity (Fig. 15) show a small scale, "monsoon-like" coupled circulation between sea and land.

Therefore, differential heating between land and sea caused by the albedo change induces a small scale coupled circulation, similar to a monsoon, in which the Mediterranean acts as a source of moisture and the orography of the Atlas enhances the upward motion. As mentioned earlier, the simple warming of the surface cannot be the only cause of the increased precipitation, but it does trigger deep convection into an environment that already has some elements that are favorable for its development. In the case of the Atlas, the favorable condition is the appropriate position of the mountain range, which can enhance orographic uplift of the flow from the Mediterranean Sea.

7. Conclusions

A high resolution (R40) global model was used to address the following question: did 2000 years of farming and cattle grazing around the Mediterranean region change the land surface properties so much as to trigger a significant response in climate? We realize that, although the spectacular remains of aqueducts, bridges and thermal baths in areas that now have no water may intuitively suggest so, and despite the drying climate trend inferred through various kinds of proxies, a quantitative evaluation has been lacking. In order to perform this vegetation change experiment around the Mediterranean, we constructed an RCP vegetation map, mainly from

palynological information or, when lacking, applying the criterion of extending relict patches of surviving vegetation over homogeneous territory.

The outcome of the experiment is that the simple introduction in a GCM of the vegetation that existed in the RCP and was cleared in the following centuries, produces a significant change in climate, characterized by a northward shift of the ITCZ and a sea–land circulation over northwestern Africa. The consequence of the climate change in the RCP experiment is that the two areas in which the contradiction between modern desert conditions and past agriculture seems more striking (the Nile valley and the Atlas range) both shift to moister conditions. Furthermore, even a very large area in which the vegetation was not changed, i.e., the Sahel, experiences a change towards moister conditions as a consequence of different land surface properties around the Mediterranean.

This experiment did not include any natural change, like the solar constant or orbital parameters, because the aim was to isolate the climate change, if any, produced by human activity around the Mediterranean. Therefore, the climate effects that are simulated in the RCP experiment are exclusively due to vegetation changes caused by human action.

The control model climate, in which the RCP vegetation is not present, cannot reach some critical values of rainfall that are theoretically necessary to sustain the RCP vegetational environments over northern Africa. As stressed already, we are aware of the complexity of a subject like the sustainable vegetation, in which extreme weather events, soil chemistry and erosion, and biological factors play a major role. It must be acknowledged that the change in land surface properties is only one of many aspects of the problem. Changes in the orbital parameters, long-term ocean temperature variations and finally the capability of the vegetation to react to climate change (i.e., a "dynamical vegetation") should also be taken into account. However, the fact that the mere change in surface properties can induce a change in the model climate which is consistent with the historical and palynological records, suggests that the action of clearing might have contributed to a positive feedback on climate and a drift towards drier conditions. It is also possible that global scale forcings were favorable for such changes in the Mediterranean region and the local clearings further accentuated the global effects.

Acknowledgements

This work was supported by the National Science Foundation (ATM-93-41271), the National Oceanic and Atmospheric Administration (NA76GP0258) and the National Aeronautics and Space Administration (NAG5-4977). We thank Dr. P. Dirmeyer for his relevant contribution, Drs. U.S. Bhatt and J. Kinter for their careful review and useful comments and Prof. E. Feoli for aid in finding palynological information.

References

Bell, M., Walker, M.J.C., 1992. Late Quaternary Environmental Change. Wiley, New York.

Birks, H.J., Birks, H.H., 1980. Quaternary Paleoecology. Edward Arnold, London.

Buzzi, A., Tibaldi, S., 1978. Cyclogenesis on the lee of the Alps: a case study. Q. J. R. Meteorol. Soc. 104, 271–287.

Dirmeyer, P.A., 1992. GCM Studies of the influence of vegetation of the general circulation: the role of albedo in modulating climate change. PhD Thesis, Univ. of Maryland, 227 pp.

Dirmeyer, P.A., Shukla, J., 1994. Albedo as a modulator of climate response to tropical deforestation. J. Geophys. Res. 99, 863–877.

Dorman, J.L., Sellers, P.J., 1989. A global climatology of albedo, roughness length and stomatal resistance for atmospheric general circulation models as represented by the simple biosphere model (SiB). J. Appl. Meteorol. 28, 834–855.

Fantechi, R., Margaris, N.S., 1986. Desertification in Europe. Symposium on climatology, Mytilene, Greece, 1984. D. Reidel Publishing, 231 pp.

Fennessy, M.J., Shukla, J., 1999. Impact of initial soil wetness on seasonal atmospheric prediction. J. Climate 12, 3167–3180.

Floret, C., Le Floc'h, M., Pontanier, R., Romane, F., 1980. Desertification in the Oglat Merteba region, Tunisia. Case Study presented by the Government of Tunisia. In: Case Studies on Desertification. United Nations Educational, Scientific and Cultural Organization (UNESCO), pp. 1–51.

Grove, A.T., 1972. Climatic change in Africa in the last 20000 years, Colloque de Ouarghla (Sept. 1971). Les Problems de Development du Sahara Septentrional, (Development Problems of Northern Sahara, in French), Algiers, Vol. 2.

Hill, M.O., 1979. TWINSPAN — A FORTRAN Program for Arranging Multivariate Data in an Ordered Two-Way Table by Classification of the Individuals and Attributes. Cornell University, Ithaca, NY.

Hooghiemstra, H., 1988. Palynological records from northwest African marine sediments: a general outline of the interpretation of the pollen signal. Philos. Trans. R. Soc. London B-318, 431–449.

Huntley, B., 1988. Europe. In: Vegetation History. Kluwer Academic Publishers, pp. 341–383.

Huntley, B., 1990. European vegetation history: paleovegetation maps from pollen data — 13000 years BP to present. J. Quat. Sci. 5, 103–122.

Huntley, B., Birsk, H.J.B., 1983. An Atlas of Past and Present Pollen Maps of Europe 0–13000 years ago. Cambridge Univ. Press.

Kinter, J.L. III, DeWitt, D., Dirmeyer, P., Fennessy, M.J., Kirtman, B.P., Marx, L., Schneider, E.K., Shukla, J., Straus, D.M., 1997. The COLA atmosphere–biosphere general circulation model. Vol. 1: Formulation. COLA Technical Report 51, 1–44.

Kinter, J.L. III, Shukla, J., Marx, L., Schneider, E.K., 1988. A simulation of the winter and summer circulations with the NMC global circulation model. J. Atmos. Sci. 45, 2486–2522.

Lamb, H.H., 1977. Climate. Present, Past and Future, Vol. 2. Barnes and Noble, 802 pp.

Lamb, H.H., 1982. Climate History and the Modern World. Cambridge University, 387 pp.

Lezine, A.M., Bonnefille, R., 1982. Holocene pollen diagram of a well at Lake Abiyata (Ethiopia, 7 degrees 42 minutes north). Polen et spores (Pollen and spores, in French) 24 (3–4), 463–480.

Lippi, M., Mariotti, M., Mercuri, A., 1992. Palynology of a resin from an Egyptian coffin of the second century B.C. Rev. Paleobot. Palynol. 71, 207–218.

Mabbutt, J.A., Floret, C., 1980. Case Studies on Desertification. UNESCO, Paris.

Mehringer, P.J., Petersen, K.L., Hassan, F.A., 1979. A pollen record from Birket Qarun and the Recent History of the Fayum, Egypt. Quat. Res. 11 (2), 238–256.

Mensching, H.G., 1986. Desertification in Europe? A Critical Comment with Examples from Mediterranean Europe. In: Desertification in Europe. Symposium on Climatology, Mytilene, Greece, 1984.. D. Reidel Publishing, pp. 3–8.

Mintz, Y., Walker, G.K., 1993. Global fields of soil moisture and land surface evapotranspiration derived from observed precipitation and surface air temperature. J. Appl. Meteorol. 32, 1305–1334.

Moore, P.D., Webb, J.A., 1978. An Illustrated Guide to Pollen Analysis. Hodder and Stoughton, London.

Nobre, C., Sellers, P., Shukla, J., 1991. Amazonian deforestation and regional climate change. J. Climate 4, 957–988.

Otterman, J., 1989. Enhancement of surface–atmosphere fluxes by desert-fringe vegetation. Theor. Appl. Climatol. 40, 67–70.

Otterman, J., 1992. Simulation of desert-scrub growth: a forcing to warmer and more pluvial climate. Adv. Atmos. Sci. 9, 441–450.

Otterman, J., Tucker, C.J., 1985. Satellite measurements of surface albedo and temperature in semi desert. J. Climate Appl. Meteorol. 24, 228–235.

Paepe, R., 1986. Landscape Changes in Greece as a Result of changing Climate during the Quaternary. In: Desertification in Europe. Symposium on Climatology, Mytilene, Greece, 1984. D. Reidel Publishing, pp. 49–58.

Reale, O., 1996. Modeling the effects on climate caused by the changes in vegetation from the Roman Classical Period. PhD Thesis, Univ. of Maryland, 163 pp.

Reale, O., Dirmeyer, P., 2000. Modeling the effects of vegetation Mediterranean climate during the Roman Classical Period. Part I: Climate History and Model Sensitivity. Global Planet. Change, 25.

Ritchie, J.C., 1987. A Holocene pollen record from Bir Atrun, northwest Sudan. Polen et spores (Pollen and spores, in French) 29 (4), 391–410.

Ritchie, J.C., Haynes, C.V., 1987. Holocene vegetation zonation in the Eastern Sahara. Nature 330 (6149), 645–647.

Speranza, A., Buzzi, A., Trevisan, A., Malguzzi, P., 1985. A theory of deep cyclogenesis in the lee of the Alps: Part I. Modification of baroclinic instability by localized topography. J. Atmos. Sci. 42, 1521–1535.

Van Overloop, E., 1986. Comparison of climatic evolution during postglacial times in Greece, tropical and subtropical regions, in relation to desertification. In: Desertification in Europe. Symposium on Climatology, Mytilene, Greece, 1984. D. Reidel Publishing, pp. 59–72.

Xue, Y.-K., Sellers, P.J., Kinter, J.L., Shukla, J., 1991. A simplified biosphere model for global climate studies. J. Climate 4, 345–364.